Genetic code expansion, click chemistry, and light-activated PI3K reveal details of membrane protein trafficking downstream of receptor tyrosine kinases

Duk-Su Koh*[1], Anastasiia Stratiievska*[1], Subhashis Jana[2], Shauna C. Otto[1], Teresa M. Swanson[1], Anthony Nhim[1], Sara Carlson[1,5], Marium Raza[1], Lígia Araujo Naves[1,6], Eric N. Senning[3], Ryan A. Mehl[2], Sharona E. Gordon[1,4]

*contributed equally to the work

[1]University of Washington, Department of Physiology & Biophysics

[2]Department of Biochemistry and Biophysics, Oregon State University

[3]Department of Neuroscience, University of Texas at Austin

[4]Address correspondence to: Sharona E. Gordon, University of Washington, 206-679-4229, seg@uw.edu

[5]Present Address: Allen Institute for Cell Sciences, Seattle, WA

[6]Present Address: Instituto de Ciências Biológicas, Universidade Federal de Minas Gerais, Belo Horizonte, Brazil

ABSTRACT

Ligands such as insulin, epidermal growth factor, platelet derived growth factor, and nerve growth factor (NGF) initiate signals at the cell membrane by binding to receptor tyrosine kinases (RTKs). Along with G-protein coupled receptors, RTKs are the main platforms for transducing extracellular signals into intracellular signals. Studying RTK signaling has been a challenge, however, due to the multiple signaling pathways to which RTKs typically are coupled, including MAP/ERK, PLCγ, and Class 1A phosphoinositide 3-kinases (PI3K). The multi-pronged RTK signaling has been a barrier to isolating the effects of any one downstream pathway. Here, we used optogenetic activation of PI3K to decouple its activation from other RTK signaling pathways. In this context, we used genetic code expansion to introduce a click chemistry noncanonical amino acid into the extracellular side of membrane proteins. Applying a cell-impermeant click chemistry fluorophore allowed us to visualize delivery of membrane proteins to the plasma membrane in real time. Using these approaches, we demonstrate that activation of PI3K, without activating other pathways downstream of RTK signaling, is sufficient to traffic the TRPV1 ion channels and insulin receptors to the plasma membrane.

INTRODUCTION

Receptor tyrosine kinases activate phosphoinositide 3-kinase

Receptor tyrosine kinases (RTKs) are the second largest class of cell surface receptors, with 58 members in the human genome (Robinson et al., 2000). Binding of agonists, typically polypeptides such as growth factors, to their extracellular amino-terminal domains results in autophosphorylation of their intracellular carboxy-terminal domains (Lemmon and Schlessinger, 2010). The autophosphorylated receptors then signal to activate phospholipase Cγ, mitogen activated protein kinase, and phosphoinositide 3-kinase (PI3K). The complex web of signals downstream of RTKs underlies their importance in a cell regulation and dysregulation but also makes studying the roles and dynamics of any particular branch of their signaling pathways challenging.

The Class IA phosphoinositide 3-kinases (PI3K) coupled to RTKs are obligate heterodimers composed of regulatory p85 and catalytic p110 subunits (Figure 1A) (Geering et al., 2007). The p85 regulatory subunit contains two SH2 domains (N-SH2 and C-SH2) separated by an inter-SH2 domain (iSH2). The p110 catalytic subunit interacts with the entire N-SH2-iSH2-C-SH2 region of PI3K, with the N-SH2 acting as an autoinhibitory domain to inhibit catalysis. For the well studying RTK tropomyosin receptor kinase A (TrkA), binding of its agonist nerve growth factor (NGF) triggers autophosphorylation of a pair of tyrosines. Phospho-TrkA then binds to the PI3K N-SH2. This has the dual effect of recruiting PI3K to the PM (Thorpe et al., 2015; Ziemba et al., 2016) and causing a conformational change in p85 to relieve auto-inhibition of p110 by the N-SH2 (Zhang et al., 2020). Activation of the RTK insulin receptor (InsR) by its agonist, insulin, also involves autophosphorylation of tyrosines on its intracellular domain and subsequent activation of PI3K; however, in the case of InsR, various insulin receptor substrate adaptor proteins link InsR to PI3K (Ye et al., 2017; Saltiel, 2021). PI3K bound directly or indirectly to activated RTKs on the membrane then phosphorylates phosphoinositide 4,5-bisphosphate ($PI(4,5)P_2$) to generate phosphoinositide 3,4,5-trisphosphate ($PI(3,4,5)P_3$).

$PI(3,4,5)P_3$ is a well-recognized signal for membrane fusion in organisms ranging from *dictyostelium* (Nichols et al., 2015) to humans (Hawkins et al., 2006; Hawkins and Stephens, 2015). Indeed, $PI(3,4,5)P_3$-triggered membrane fusion mediates tumor cell motility, with PI3K acting as an oncoprotein and its corresponding phosphatase, PTEN, as a tumor suppressor (Hawkins et al., 2006).

RTK/PI3K signaling increases sensitivity to painful stimuli via TRPV1 ion channels

Increased sensitivity to painful stimuli in injured and inflamed tissue is due to adaptations in the peripheral and central nervous systems (McMahan et al., 2013). For peripheral sensitization, G-protein coupled receptors and RTKs signal through multiple pathways to produce cellular changes across multiple time scales. NGF is an inflammatory mediator released from leukocytes, including mast cells, eosinophils, macrophages, and lymphocytes, in response to tissue injury and inflammation (Freund-Michel and Frossard, 2008; Reis et al., 2022). Paradoxically, in addition to its role increasing sensitivity to painful stimuli, NGF also is critical for wound healing (Ebadi et al., 1997; Lambiase et al., 2000; Bonini et al., 2002). Thus, strategies to block NGF-mediated pain sensitization have the unfortunate consequence of interfering with post-injury recovery.

One of the mechanisms by which NGF increases sensitivity to pain involves a PI3K-induced increase in the number of pain-transducing TRPV1 ion channels in the plasma membrane (PM) of sensory neurons (Bonnington and McNaughton, 2003; Stein et al., 2006; Zhu and Oxford, 2007). We recently discovered reciprocal regulation between TRPV1 and PI3K. We found that the NGF-stimulated rise in the PI3K product $PI(3,4,5)P_3$ is much greater in cells transiently transfected with TRPV1 than in control cells without TRPV1, i.e., TRPV1 enhances NGF-mediated PI3K activity (Stratiievska et al., 2018). Interestingly, TRPV1 interacts directly with PI3K (p85α and p85β subunits; Figure 1A) via its amino-terminal ankyrin repeat domain (ARD) (Stein et al., 2006) and the ARD is sufficient to increase NGF-induced PI3K activity (Stratiievska

et al., 2018). Based on these findings, we propose that TRPV1 regulates NGF-induced PI3K activity via this direct interaction.

Insulin/PI3K signaling

Activation of InsR by insulin signals via PI3K to activate a powerful protein kinase, Akt, which in turn regulates multiple cellular processes involved in metabolism (Saltiel, 2021). The PI3K/Akt pathway is thus of great interest in understanding obesity and type 2 diabetes. Insulin-dependent recycling of InsR has also been extensively studied (Knutson, 1991; Chen et al., 2019). Ligand-simulated InsR endocytosis is followed by either targeting to lysosomes for degradation or recycling endosomes for reinsertion into the PM. This return to the PM is not fully understood, but it is believed to involve small Rab family GTPases (Iraburu et al., 2021). Importantly, pharmacological inhibition of PI3K has been shown to inhibit InsR trafficking to the PM, indicating that PI3K activity is necessary for InsR homeostasis (Sasaoka et al., 1999).

Approaches to studying membrane protein trafficking

The properties of conventional fluorescent labels have posed a significant barrier to understanding trafficking of membrane proteins, including TRPV1. Previous studies have used large tags to label the channel protein, typically a fluorescent protein (e.g., GFP) fused to the intracellular N- or C-terminus. Fusion to fluorescent proteins carries a number of disadvantages. Fluorescent proteins are relatively dim and are susceptible to bleaching. We and others have previously shown that the intracellular termini participate in critical protein-protein interactions, some of which are involved in channel trafficking (Morenilla-Palao et al., 2004; Stein et al., 2006; Jeske et al., 2008; Camprubi-Robles et al., 2009; Jeske et al., 2009; Xing et al., 2012; Gregorio-Teruel et al., 2015; Mathivanan et al., 2016; Meng et al., 2016). The presence of large fluorescent proteins could perturb these interactions (Tsien, 1998; Montecinos-Franjola et al., 2020). TRPV1 is expressed heavily in intracellular membranes, making it nearly impossible to optically isolate just those channels on the PM (Liu et al., 2003; Gallego-Sandín et al., 2009).

Fluorescent anti-TRPV1 antibodies have been used to label extracellular epitopes to distinguish these populations (e.g., (Meng et al., 2016; Nakazawa et al., 2021)), but antibodies have the same problem of large size, and we have found that antibodies that recognize extracellular regions of TRPV1 are not very specific.

Click chemistry offers a rapid, specific, and flexible method for labeling of proteins in living cells (Lang and Chin, 2014; Nikić et al., 2015; Kenry and Liu, 2019). We have previously incorporated click chemistry-compatible noncanonical amino acids (ncAAs) into amino acid positions in the cytoplasm of mammalian cells and shown we can achieve highly efficient and rapid labeling when introducing the appropriate click chemistry probe into the medium (Jang et al., 2020; Jana et al., 2023). This approach requires co-expression of the target gene with an amber stop codon (TAG) with a plasmid encoding an evolved aminoacyl tRNA synthetase that is orthogonal to mammalian cells, together with its cognate tRNA (Chin, 2014; Uttamapinant et al., 2015). An additional plasmid encoding a dominant negative form of eukaryotic dominant negative elongation release factor can be expressed to increase efficiency of ncAA incorporation (Schmied et al., 2014). Incorporating a click chemistry ncAA into an extracellular position in a membrane protein and then applying a membrane-impermeant click chemistry-conjugated fluorophore would allow specific labeling of protein at the surface, even for those proteins that localize to both the surface and intracellular membranes (Gregory et al., 2016; Mateos-Gil et al., 2016; Neubert et al., 2018; Ojima et al., 2021). The recent development of click chemistry ncAAs and fluorescent probes that react very rapidly ($>10^4$ $M^{-1}s^{-1}$) make this an attractive approach for tracking membrane protein trafficking in real time (Peng and Hang, 2016; Row and Prescher, 2018; Meineke et al., 2020; Jana et al., 2023).

In this work, we leverage optogenetics to activate PI3K with light, genetic code expansion to incorporate a click chemistry ncAA, and a new, membrane-impermeant click chemistry-conjugated fluorophore to interrogate the mechanism by which NGF induces trafficking of

TRPV1 to the PM. By isolating the PI3K pathway downstream of NGF from the other pathways coupled to TrkA (PLCγ and MAP/ERK), we demonstrate that PI3K activity is sufficient to increase TRPV1 trafficking to the PM. We apply the same approach to InsR, to demonstrate that our new approach is of general use for different types of membrane proteins, and show that activation of PI3K is sufficient to increase InsR trafficking to the PM. Given the importance of InsR recycling in the development of insulin resistance, understanding the role of PI3K in regulating InsR expression on the PM is critical.

RESULTS

Here, we used the previously published phytochrome B (PhyB)/phytochrome interacting factor (PIF) system to activate and deactivate PI3K with light (Figure 1B) (Levskaya et al., 2009; Toettcher et al., 2011). Uncoupling PI3K from activation of TrkA allowed us to study the effects of PI3K on membrane protein trafficking without activating other signaling pathways downstream of TrkA. To apply the PhyB/PIF system to control PI3K activity, we fused the inter-SH2 domain (iSH2) of the p85 regulatory subunit of PI3K to PIF (Figure 1C). It has previously been shown that the iSH2 domain associates with the endogenous p110 catalytic subunit of PI3K (Klippel et al., 1993). Because this heterodimer is missing the autoinhibitory domains of p85, it is constitutively active, so that PI3K phosphorylates its substrate, PI(4,5)P_2 to make PI(3,4,5)P_3 whenever the PIF-iSH2-YFP is driven to the membrane (Figure 1C) (Suh et al., 2006; Idevall-Hagren et al., 2012). The iSH2 domain has been previously expressed as a fusion protein with PIF and has been shown to reversibly translocate to the PM and activate PI3K in response to light (Figure 1 – figure supplement 1) (Levskaya et al., 2009; Toettcher et al., 2011).

Using a CFP-labelled pleckstrin homology domain from the enzyme Akt (Akt-PH-CFP), which specifically binds the PI(3,4,5)P_3 product of PI3K (Lemmon, 2008), as a probe for PI(3,4,5)P_3, we confirmed that the PhyB/PIF-iSH2 machinery could be used to rapidly generate PI(3,4,5)P_3 in response to 650 nm light (Figure 1D-E). In response to 750 nm light, PIF-iSH2-

YFP was released from the membrane and the levels of PI(3,4,5)P_3 returned to baseline, presumably due to the activity of the endogenous PI(3,4,5)P_3 phosphatase PTEN. Similar experiment using GRP1-PH-CFP, another PI(3,4,5)P_3 probe yielded the same results (Figure 1-figure supplement 2).

Activation of PI3K, without other pathways downstream of NGF/TrkA, is sufficient to drive trafficking of TRPV1 to the PM

We and others have previously demonstrated that activation of the RTK TrkA by nerve growth factor leads to increased trafficking of the ion channel TRPV1 to the PM (Zhang et al., 2005; Stein et al., 2006; Zhu and Oxford, 2007; Stratiievska et al., 2018) This increase in surface expression is associated with increased sensitivity to painful stimuli sensed by TRPV1. As shown in Figure 2A-B, the NGF-induced trafficking of TRPV1 follows the increase in PM PI(3,4,5)P_3 levels. Although TrkA couples with PLCγ and the MAP/ERK pathways in addition to PI3K, significant evidence indicates that PI3K activation is *necessary* to NGF-induced trafficking of TRPV1 to the PM (Zhang et al., 2005; Stein et al., 2006; Zhu and Oxford, 2007; Stratiievska et al., 2018).

We used PhyB with PIF-iSH2 to test the hypothesis that PI3K activity is *sufficient* to drive trafficking of TRPV1 to the PM. Together with PhyB, PIF-iSH2 (without a fluorescent tag) and Akt-PH-CFP, we expressed TRPV1 fused to YFP. Stimulation of cells with 650 nm light gave the expected rise in PM-associated Akt-PH-CFP fluorescence and, importantly, a rise in PM-associated TRPV1-YFP fluorescence (Figure 2C-D). The light-induced rise in PM PI(3,4,5)P_3 and TRPV1 qualitatively resembled those induced by NGF. Because PLCγ and the MAP/ERK were not directly activated by the 650 nm light, we conclude that activation of the PI3K pathway is sufficient to cause TRPV1 trafficking to the PM.

TRPV1 prevents dissociation of PIF-iSH2-YFP from the membrane in response to 750 nm light

In monitoring localization of PIF-iSH2-YFP in light-activated PI3K experiments in TRPV1-expressing cells, we found that PIF-iSH2-YFP no longer translocated to the cytoplasm in response to 750 nm light (Figure 2 – figure supplement 1A-B). Indeed, the small amount of mCherry excitation light (561 nm) used to identify PhyB-mCherry positive cells seemed to be sufficient to cause a slow accumulation of PIF-iSH2-YFP at the PM even during continuous exposure of the cell to 750 nm light (Figure 2 – figure supplement 1C-D). Not surprisingly, with PIF-iSH2-YFP accumulating at the PM during imaging of TRPV1-expressing cells, the 650 nm light-induced increase in plasma-membrane associated Akt-PH-CFP did not reverse upon exposure to 750 nm light (Figure 2C-D). TRPV1 expression had no effect on a version of PIF-YFP that lacked the iSH2 domain (Figure 2 – figure supplement 2), indicating that irreversible localization to the PM required both the iSH2 fragment of PI3K and TRPV1. Expression of the related TRPM4 ion channels, which do not include an ankyrin repeat domain, also had no effect on 750 nm light-induced dissociation of PIF-iSH2-YFP from the PM (Figure 2 – figure supplement 3), indicating that this effect is specific to TRPV1. We have previously shown that the ankyrin repeat domain of TRPV1 interacts directly with the p85 subunit of PI3K from which iSH2 is derived (Stein et al., 2006). We speculate that the PIF-iSH2-YFP in TRPV1-expressing cells might not dissociate from the PM when stimulated with 750 nm light because it encounters TRPV1 at the PM and binds to it, remaining bound to TRPV1 even after releasing PhyB.

Resolving changes in surface expression requires improved approaches

TIRF microscopy was needed to resolve the NGF- and light-induced increase in PM PI(3,4,5)P_3 levels but is a poor approach for distinguishing membrane protein localization in the PM from that in intracellular compartments (Stratiievska et al., 2018). For membrane proteins with very high endoplasmic reticulum localization, like TRPV1 (Tominaga et al., 1998), this makes any changes in fluorescence intensity measured with TIRF an underestimate of true changes in surface localization.

To circumvent contamination of TIRF signals on the PM with fluorescence from intracellular compartments, we implemented an inverse-electron-demand Diels–Alder cycloaddition click chemistry approach to selectively label PM localized proteins (Arsić et al., 2022). For this application, we used genetic code expansion to incorporate a noncanonical amino acid at an extracellular site (Neubert et al., 2018; Bessa-Neto et al., 2021; Kuhlemann et al., 2021). We used Tet3-Bu (Figure 3A), a tetrazine-containing amino acid which can be efficiently labelled with a cyclopropane-fused strained trans-cyclooctene (sTCO) with no detectable off-target reactivity within the time scale of our experiments (see below) (Jang et al., 2020; Jana et al., 2023). Our goal was to express membrane proteins incorporating Tet3-Bu at an extracellular site and measure labeling with a membrane-impermeant sTCO-coupled dye (Figure 3B) under control conditions and then again after activation of PI3K with either NGF or 650 nm light.

We tested our click chemistry/noncanonical amino acid approach using TRPV1 and the insulin receptor (InsR), a model RTK we and others have previously used in studies with different noncanonical amino acids (Nikić et al., 2015; Jones et al., 2021). For both proteins, we used amber codon suppression to site-specifically incorporate Tet3-Bu (Jang et al., 2020) into an extracellular loop (T468Tet3-Bu for TRPV1 and K676Tet3-Bu for InsR). This involved introducing a TAG stop codon at the selected site within the coding sequence that would place the noncanonical amino acid on the extracellular side of the PM. We then co-expressed one plasmid encoding either TRPV1-T468TAG or InsR-K676TAG fused to GFP, a second plasmid encoding an aminoacyl tRNA synthetase evolved to incorporate the noncanonical amino acid and the orthogonal tRNA, and a third plasmid encoding a dominant negative elongation release factor, which increased the efficiency of Tet3-Bu incorporation (Schmied et al., 2014). The cell culture medium was then supplemented with Tet3-Bu. As indicated by the GFP signal and in-gel fluorescence both TRPV1-T468Tet3-Bu-GFP and InsR-K676Tet3-Bu-GFP expressed at high levels only in transfected cells (Figure 3C,E and Figure 3 – figure supplement 1C). To test

whether incorporation of Tet3-Bu interfered with the function of TRPV1, we measured capsaicin-activated currents with whole-cell voltage clamp and found that TRPV1-T468Tet3-Bu-GFP gave robust capsaicin-activated currents (Figure 3 – figure supplement 1A-B). To determine whether InsR-K676TAG protein retained its function, we measured insulin-induced endocytosis (Carpentier et al., 1992) and found endocytosis in response to insulin was maintained (Figure 3 – figure supplement 2) with approximately the expected kinetics (Figure 3 –movie supplement 1).

Developing a membrane-impermeant sTCO dye

Strained trans-cyclooctenes bearing functional groups such as spin labels and fluorophores have been used previously for in-cell studies (Murrey et al., 2015; Ryan et al., 2022; Jana et al., 2023). To determine whether existing sTCO-conjugated dyes would give the required PM-selective labeling, we tested whether sTCO-TAMRA (Jang et al., 2020), or sTCO-JF646 (Jana et al., 2023) were membrane impermeant. We also synthesized and tested sTCO-fluorescein. Unfortunately, these compounds readily equilibrated across the cell PM at the concentrations required for labeling, giving indistinguishable cytosolic fluorescence in untransfected and transfected cells (Figure 3 – figure supplement 3A-C). We therefore synthesized a new sTCO-sulfo-Cy5 conjugate, which contains two negative charges at physiological pH to minimize passive diffusion through membrane and therefore selectively label membrane proteins at the cell surface (Figure 3 – figure supplement 3D) (Hoffmann et al., 2015; Nikić et al., 2015; Kozma et al., 2016; Lam et al., 2018; Keller et al., 2020).

To determine whether sTCO-sulfo-Cy5 would selectively label a membrane protein with an extracellular Tet3-Bu, we measured Cy5 fluorescence in the presence of 200 nM sTCO-sulfo-Cy5 in the bath, a low concentration that gives very low background fluorescence. The click chemistry reaction between Tet3-Bu incorporated at the extracellular sites and sTCO-sulfo-Cy5 effectively concentrated the dye at the PM, allowing significant membrane labeling to be

observed for both membrane proteins examined (TRPV1-T468Tet3-Bu-GFP – Figure 3C and InsR-K676Tet3-Bu-GFP – Figure 3E). Importantly, sTCO-sulfo-Cy5 did not appear to equilibrate across the cell membrane and did not label untransfected cells (i.e., those without GFP; Figure 3 – figure supplement 3D). *In vitro*, the click chemistry reaction between free Tet3-Bu ncAA and sTCO occurs with a rate of $2x10^4$ $M^{-1}s^{-1}$; this reaction rate increased by 4 fold when Tet3-Bu was incorporated on the surface of GFP (Jang et al., 2020). The low background fluorescence recorded with 200 nM dye in the bath allowed us to measure the rate of labeling for TRPV1-468Tet3-Bu-GFP and InsR-646Tet3-Bu-GFP with sTCO-sulfo-Cy5. As shown in Figure 3D-F, the reaction rate we measured was approximately $5x10^3$ $M^{-1}s^{-1}$ for both proteins, somewhat slower than expected for a protein in solution and on par with the reaction between the free amino acid and sTCO in solution (Meijer et al., 1998; Taylor et al., 2011).

Click chemistry labeling can be used to measure NGF-induced trafficking of TRPV1 to the PM

Based on the extensive contamination of TIRF signals with fluorescence from the ER and other intracellular compartments (Stratiievska et al., 2018), we hypothesized that our previous measurements of NGF-induced trafficking of TRPV1 to the PM using TIRF represent underestimates of the true changes in PM TRPV1. If this were the case, using click chemistry to resolve NGF-induced changes in PM TRPV1 should reveal a greater increase in PM TRPV1. At the beginning of the experiment, we labeled surface TRPV1-468Tet3-Bu-GFP with a pulse of 1 μM sTCO-sulfo-Cy5 and then washed the label from the bath (Figure 4A). We used this higher concentration of sTCO-dye (5 times higher than in Figure 3) to label the PM channels more rapidly, as the NGF-induced trafficking of TRPV1 to the PM occurs with kinetics comparable to labeling with 200 nM sTCO-sulfo-Cy5 (compare Figure 2A to Figure 3D). We then treated the cells with NGF for ten minutes and again pulse labelled the surface channels with a brief exposure to 1 μM sTCO-sulfo-Cy5. We observed a ~1.4 fold increase in PM Cy5 staining, indicating that NGF induced trafficking of TRPV1 to the surface (Figure 4B-D). In contrast, the

total number of TRPV1 channels did not change, as evidenced by the total intensity of GFP fluorescence, which was not affected by NGF. This NGF-induced increase in surface expression is indeed greater than the ~1.1-fold increase in NGF-induced surface expression of TRPV1 observed in TIRF experiments (Figure 2A-B). In control experiments in which cells were exposed to the vehicle (without NGF), neither the GFP signal nor the sTCO-sulfo-Cy5 signal changed (Figure 4E), indicating that the NGF-induced increase in sTCO-sulfo-Cy5 was specific to activation of the TrkA receptor by NGF.

Click chemistry labeling can be used to measure light-induced trafficking to the PM

We next asked whether click chemistry labeling could improve the resolution of PM trafficking in a system in which we have decoupled PI3K activity from other pathways downstream of NGF, i.e., the PhyB/PIF system. Results from these experiments with TRPV1-468Tet3-Bu-GFP and InsR-676Tet3-Bu-GFP and shown in Figure 5. After first labeling cells with sTCO-sulfo-Cy5, we exposed cells to an initial 10-minute exposure to 750 nm light and labeled any newly delivered protein at the PM using a second treatment with sTCO-sulfo-Cy5 (Figure 5A). The GFP fluorescence remained the same under all conditions indicating that total protein expression did not change over the course of the experiments. For TRPV1-T468Tet3-Bu-GFP, the sTCO-sulfo-Cy5 labeling increased slightly in response to the initial exposure to 750 nm light (Figure 5B, D). This small increase in sTCO-sulfo-Cy5 labeling was specific to TRPV1-T468Tet3-Bu, as 750 nm light produced no change in sTCO-sulfo-Cy5 labeling of InsR-K676Tet3-Bu-GFP (Figure 5F, H). The TRPV1-specific increase in labeling after 750 nm illumination is likely due to the small, irreversible PM localization of PIF-iSH2-YFP that occurs in TRPV1-expressing cells (Figure 2 – figure supplement 1). This small increase in sTCO-sulfo-Cy5 labeling of TRPV1-T468Tet3-Bu was also seen in control experiments using two sequential exposures to 750 nm light (Figure 5 – figure supplement 1). Note that the increase in of TRPV1-T468Tet3-Bu labeling, F_2/F_1, in

experiments with 650 nm light (Figure 5) was significantly greater than F_2/F_1 in experiments with only 750 nm light ($P < 0.001$; Figure 5 – figure supplement 1).

After the initial control period with 750 nm light, we exposed the cells to 650 nm light for 10 minutes to activate PI3K and then labeled newly delivered protein at the PM with sTCO-sulfo-Cy5. As shown in Figure 5B-E for TRPV1-T468Tet3-Bu and Figure 5F-I for InsR-K676Tet3-Bu-GFP, activation of PI3K with 650 nm light increased expression of protein on the PM. For TRPV1, the amplitude of the increase in surface expression, ~1.4-fold, was similar to that observed in click chemistry experiments in response to NGF (Figure 4). Surprisingly, the increase in surface expression of InsR-K676-Tet3-Bu was also about 1.4-fold. Like the NGF receptor TrkA, InsR is a receptor tyrosine kinase whose activation stimulates PI3K activity (Saltiel, 2021). Binding of insulin to InsR is a well-studied signal for InsR endocytosis (Carpentier et al., 1992), and PI3K activation downstream of InsR is key to delivery of GLUT4 transporters to the PM (Saltiel, 2021). However, to our knowledge, PI3K activity has not been previously known to stimulate InsR delivery to the PM. Although it would be exceedingly interesting if insulin binding to InsR could trigger both InsR endocytosis *and* exocytosis, further studies will be required to determine the physiological significance, if any, of PI3K-stimluated delivery of InsR to the PM.

DISCUSSION

Here, we present proof-of-principle experiments demonstrating the simultaneous use of an optogenetic approach for PI3K activation and genetic code expansion/click chemistry to interrogate regulation of membrane protein trafficking. This combination of approaches is especially useful for membrane proteins with significant expression in the endoplasmic reticulum and/or other intracellular compartments, which makes it very difficult to identify proteins in the PM definitively when using fusions with GFP or similar genetically encoded labels. In addition to distinguishing proteins at the surface, using a small ncAA and click chemistry is likely much less

perturbing to protein structure and function than fusion with a ~20-30 kDa protein such as GFP, SNAP-tag or HaloTag. Restricting the ncAA and fluorescent label to an extracellular region/loop is also less likely to interfere with protein-protein interactions on the intracellular side, compared with a large protein fusion to an intracellular N- or C-terminal of a protein of interest.

Successful implementation of this approach required overcoming a number of barriers: efficient incorporation of Tet3-Bu into the extracellular sites; demonstration that the Tet3-Bu-incorporating protein had the expected functional properties; development of a membrane impermeant sTCO-coupled dye; and optimization of the PhyB/PIF and genetic code expansion machinery in the same cells. Incorporation of Tet3-Bu at the extracellular side of TRPV1 was well tolerated in the S1-S2 loop, with two of four sites yielding functional, capsaicin-activated channels. We have found incorporation efficiency to be difficult to predict. Screening through desirable sites typically is the best approach, with approximately one half to one third of selected sites showing reasonable levels of ncAA incorporation.

There is significant room for improvement of these methods, particularly in developing more rapid labeling of the ncAA. As shown in Figure 3, complete labeling with a low concentration of sTCO-dye required more than 10 minutes. Monitoring membrane protein trafficking to the surface in real time will require a reaction that is at least five- to 10-fold faster. Increasing the speed of labeling can be accomplished using ≥1 μM sTCO-dye, but at such high concentrations of dye the background signal from dye in solution interferes with imaging. We have recently developed new ncAAs with the tetrazine ring more proximal to the amino acid beta carbon, which we term Tet4, that react with sTCO-based labels with rates as fast as 10^6 $M^{-1}s^{-1}$ (Jana et al., 2023). The aminoacyl tRNA synthetases that incorporate Tet4 amino acids into mammalian cells are not as efficient as those for Tet3 amino acids. Improving the efficiency of incorporating Tet4 amino acids would allow us to express Tet4-incorporating proteins and measure delivery of proteins to the PM in real time.

Another limitation to our approach is the need to co-express five to six plasmids to use PhyB/PIF and Tet/sTCO machinery simultaneously. Developing stable cell lines for ncAA incorporation would reduce the need for multiple plasmid transfection and, perhaps, lead to more uniform expression across cell populations. The PhyB/PIF machinery requires supplementing cell medium with the phycocyanobilin (PCB) chromophore, making it incompatible with *in vivo* experiments. Introducing four genes, PcyA, H01, Fd, and Fnr, and knocking down/out biliverdin reductase A leads to efficient synthesis of phycocyanobilin in mammalian cells (Uda et al., 2017; Uda et al., 2020). It is therefore possible that genetically modified animals might one day express the PhyB/PIF machinery and chromophore and allow optogenetic activation of PI3K *in vivo*. However, there is as yet no method for synthesizing the necessary ncAAs within cells, precluding *in vivo* use of the PhyB/PIF with tetrazine-based genetic code expansion.

PI3K is a universal signal for trafficking to the PM. In *dictyostelium*, PI3K activation at the leading edge of cells underlies chemotaxis towards nutrients (Nichols et al., 2015). In macrophages, PI3K at the leading edge of cells drives motility towards the object of phagocytosis (Hawkins et al., 2006; Hawkins and Stephens, 2015). In the cases discussed here, membrane proteins constitute the cargo delivered to the PM in response to PI3K signaling. A vast literature has examined the mechanisms by which InsR is recycled from the PM in response to insulin (Knutson, 1991; Ye et al., 2017; Chen et al., 2019), but less is known about ways in which delivery of InsR to the PM is regulated. We show here, for the first time, that activation of PI3K is sufficient to increase InsR in the PM. Future studies will be needed to understand the role for this process in liver and muscle cells. For TRPV1, PI3K was identified as an important signal that enhances surface expression in response to nerve growth factor, but the steps between PI3K activation and fusion of vesicles containing TRPV1 cargo with the PM

are a mystery. The tools developed here provide a means by which the cellular mechanisms underlying PI3K-mediated delivery of membrane proteins can be interrogated.

MATERIALS AND METHODS

Molecular Biology and Constructs Used

The cDNAs used in this study were provided by: rat TRPV1 in pcDNA3.1 – David Julius, UCSF, San Francisco, CA (Caterina et al., 1997); the human insulin receptor (accession AAA59452.1) with the K676TAG mutation and C-terminal GFP in a plasmid based on pEGFP– Edward Lemke, European Molecular Biology Laboratory (EMBL), Heidelberg, Germany (Nikić et al., 2015); eukaryotic elongation release factor 1 with E55D mutation in pCDNA5-FRT– Jason Chin, Medical Research Council Laboratory of Molecular Biology, Cambridge, England (Schmied et al., 2014); TrkA (rat) in the pcCMV5 vector and p75NTR (rat) in the pcDNA3 vector from Mark Bothwell, University of Washington, Seattle, WA; PH-Akt-cCerulean in pcDNA3-k vector- Orion Weiner, UCSF, San Francisco, CA (Toettcher et al., 2011) and *Methanosarcina barkeri* R2–84-RS aminoacyl tRNA synthetase/$tRNA_{CUA}$ in the pAcBac1 plasmid – Ryan Mehl, University of Oregon, Corvallis, OR (Jang et al., 2020). Gibson cloning was used to generate the C-terminal GFP fusion for TRPV1 and to introduce 468TAG stop codon. All constructs were verified using Sangar sequencing.

In selecting the extracellular site for ncAA incorporation into TRPV1, we focused on the S1-S2 loop (Figure 3C) because the S3-S4 loop is very short (5 amino acids) and we wished to avoid the pore turret between S5 and S6, which has been implicated in gating of the pore (Yang et al., 2015; Bae et al., 2016; Jara-Oseguera et al., 2016; Ma et al., 2016). In our initial screen, we tested incorporation at four positions, R455, V457, K464 and T468 (Figure 3C) and used a C-terminal GFP fusion to facilitate screening. We found that TRPV1-K464Tet3-Bu-GFP and TRPV1-T468Tet3-Bu-GFP produced robust, capsaicin-activated currents when interrogated with whole-cell patch-clamp Figure 3– figure supplement 1A-B), whereas TRPV1-R455Tet3-Bu-GFP and TRPV1-V457Tet3-Bu-GFP of incorporation did not (data not shown). We focused on TRPV1-T468Tet3-Bu-GFP, as TRPV1-K464Tat3-Bu-GFP was not efficiently labelled in

subsequent experiments (data not shown). We next tested whether expression of full-length TRPV1-T468Tet3-Bu-GFP required incorporation of Tet3-Bu using in-gel GFP fluorescence. As shown in Figure 3 – figure supplement 1C, detergent solubilized cell lysates from cells expressing TRPV1-T468Tet3-Bu-GFP showed a band at the expected molecular weight when the medium was supplemented with Tet3-Bu, but no GFP fluorescence at this molecular weight was observed when the medium lacked Tet3-Bu. These data indicate that TRPV1-T468Tet3-Bu-GFP incorporated Tet3-Bu without measurable incorporation of natural amino acids at the TAG codon site.

Cell Culture/transfection/solutions

The experiments in Figure 1 were performed in an NIH/3T3 cell line stably expressing PhyB-Cherry-CAAX, PIF-iSH2-YFP, and Akt-PH-CFP. These cells were a gift from Orion Weiner (UCSF, San Francisco, CA). NIH-3T3 cells were cultured at 37°C, 5% CO_2 in Dulbecco's modified Eagle's medium (Invitrogen, Grand Island, NY) supplemented with 10% bovine calf serum (Hyclone, Logan, UT), L-Glutamine (Invitrogen), and penicillin/streptomycin (Lonza, Switzerland).

F-11 cells (a gift from M.C. Fishman, Massachusetts General Hospital, Boston, MA; (Francel et al., 1987)), a hybridoma of rat dorsal root ganglion neurons and mouse neuroblastoma cells, were used for experiments in Figures 1, 2, and Figure 3-figure supplement 2, as they are an appropriate model for studying NGF-induced signaling in pain receptor neurons. F-11 cells were incubated in Ham's F-12 Nutrient Mixture (Gibco) supplemented with 20% fetal bovine serum, penicillin/streptomycin, and HAT supplement (100 μM sodium hypoxanthine, 400 nM aminopterin, 16 μM thymidine; Invitrogen). Click chemistry experiments in Figures 3 through 6 were performed in HEK293T/17 cells (Catalog #CRL-11268, ATCC, Gaithersburg, MD) because

these cells are optimized for transfection with multiple plasmids. HEK293T/17 cells were incubated according to manufacturer's instructions in DMEM supplemented with 10% fetal bovine serum and penicillin/streptomycin.

Cells were transfected using Lipofectamine 2000 (Invitrogen) or JetPrime (Polyplus, Illkirch, France) according to the instructions of the manufacturers. Cells were passaged on to 25-mm round glass coverslips (Warner Instruments, Hamden, CT) 12 hours after transfection and cultured until used for experimentation 16–48 hours later. The coverslips were coated with poly-L-lysine to aid cell attachment (Sigma-Aldrich, St. Louis, MO .3For the optogenetic system, HEK293T/17 cells were transfected with PhyB-mCherry-CAAX (5 µg/well in 6-well culture plate), PIF-ISH2-YFP (or PIF-YFP) 0.5 µg. The 10:1 ratio helped to express more PhyB membrane target and lesser amount of PIF cargo. When cytoplasmic PIF-ISH2-YFP was highly expressed, its translocation toward the PM upon activating 650 nm light appeared significantly reduced, likely due to the difficulty of separating signal in the cytoplasm from that at the PM. For expression of TAG-encoding cDNAs, HEK293T/17 cells in 6-well plates at 30-50% confluency were transfected target gene cDNAs at 2:1 ratio (proteins with TAG codon: RS 2-84), with a total of 2 µg/well. Dominant negative elongation release factor (DN-eRF-E55D; 0.4 µg) was added to reduce truncation of the protein at the TAG codon (Schmied et al., 2014). For NGF stimulation, F-11 cells were transfected with 1 µg each of TrkA and p75NTR along with 1 µg TRPV1 constructs. For other constructs, 1-3 µg cDNA was used for transfection. During experiments, cells were perfused with Ringer's solution (in mM: 140 NaCl, 4 KCl, 1 $MgCl_2$, 1.8 $CaCl_2$, 10 HEPES and 5 glucose, pH 7.3). All experiments were performed at room temperature except Figure 3-figure supplement 2.

Optogenetic experiments

Cells were incubated in the dark with 10 µM PCB in the culture medium for at least 1 hour prior to experiments. To avoid photodamage of Opto3K, handling of cells during and subsequent to

PCB loading was performed in the dark room using a green safety flashlight (Levskaya et al., 2009). Note that PhyB loaded with PCB is extremely sensitive to light, light of any wavelength between 560 and 650 nm can activate Phytochrome B once PCB is added (Braslavsky et al., 1997; Katrin Anders, 2015). Therefore, experiments were carried out in the presence of 750 nm deactivating light and care was taken to avoid (or minimize) the exposure of cells to 560-650 nm illumination from microscopy or the external environment, including the computer monitor.

TIRF and confocal imaging

The total internal fluorescence (TIRF) imaging set up was as described previously (Stratiievska et al., 2018). We used an inverted microscope (Nikon Ti-E) equipped with a 60x TIRF objective (NA 1.49). For activating/deactivating opto-PI3K with light, we used HQ630/20 X (42490) and HQ760/40 X (226723) excitation filters inserted in the overhead condenser filter slider. The whole experimental chamber was illuminated with activating or deactivating light using the maximum intensity (100 W at full spectrum) of the condenser lamp. Light intensity at the focal plane was 2.4 mW and 3.7 mW for 650 nm and 750 nm illumination, respectively.

Cyan Fluorescent Protein (CFP) fusion proteins were imaged using excitation from a 440 nm laser and a 480/40 nm emission filter. Yellow Fluorescent Protein (YFP) fusion proteins were monitored using the 514 nm line of an argon laser and a 525/50 nm emission filter. mCherry was excited at 561 nm and fluorescence was collected with 605/70 nm emission filter.

Time-lapse images were obtained every 10 or 20 seconds using either a QuantEM or an Evolve EMCCD camera (Photometrics). Movies were then processed using ImageJ software (NIH) (Rasband, 1997; Schneider et al., 2012). Regions of interest (ROI) were drawn around the footprint of individual cells and the average ROI pixel intensity was measured. Background fluorescence from cell-free areas were subtracted. Measurements were analyzed using Excel (Microsoft, Redmond, WA) and Igor Pro (Wavemetrics, Portland, OR). Traces were normalized by the average intensity during 1 or 3 min time period prior to activating 650 nm light.

The confocal images were obtained with a Zeiss 710 confocal microscope (Zeiss, Oberkochen, Germany). Illumination of 650-750 nm lights were controlled as described for TIRF microscopy experiments. CFP, YFP, mCherry, and JF646 were excited with 440, 514, 561, 633 nm lasers, respectively. Data were analyzed with ImageJ. The lookup table of images were changed during analysis, but the same range was applied for all images within a time series experiment.

Electrophysiology

Currents were recorded using the standard patch clamp technique (Hamill et al., 1981). Borosilicate glass electrodes had a resistance of 3–6 MΩ when filled with internal solution (in mM; 140 KCl, 5 NaCl, 0.1 EGTA, and 10 HEPES, pH 7.3). Ringer's saline was used in the extracellular bath solution. Current through ion channels was measured in whole-cell configuration and the membrane potential was held at −60 mV. To activate TRPV1, the agonist capsaicin was applied for 10 seconds using a local perfusion system which allowed the solution to exchange within 1 second (Koh and Hille, 1997). Currents were recorded with an EPC-9 amplifier (HEKA Elektronik, Lambrecht (Pfalz), Germany) and analyzed using Igor Pro software.

Endocytosis of insulin receptor

F-11 cells expressing InsR-K676TAG-GFP were treated with 30 μM Tet3.0-Bu in the culture medium for 24 hours, transferred to glass coverslip, and further cultured in serum-deprived medium for 24 hrs. The receptor targeted to the plasma membrane was labeled with membrane-impermeable sTCO-Cy3B dye (Figure 3 – figure supplement 2C) for 4 min and free dye molecules were washed with saline solution for 2 min. Confocal images were obtained every 20 s with excitation at 561 nm and emission between 600 and 640 nm. Labeling of the receptor and insulin treatment were performed at around 35 ^{o}C to promote the rate of endocytosis using a local perfusion system with heat exchanger (Koh et al., 2011).

Chemical synthesis

All purchased chemicals were used without further purification. Thin-layer chromatography (TLC) was performed on silica 60F-254 plates. Flash chromatographic purification was done on silica gel 60 (230-400 mesh size). ^{1}H NMR spectra were recorded at Bruker 400MHz. The chemical shifts, shown in ppm, are referenced to the residual nondeuterated solvent peak CD_3OD (δ =3.31 in ^{1}H NMR) as an internal standard. Splitting patterns of protons are designated as follows: s-singlet, d-doublet, t-triplet, q-quartet, quin-quintet, m-multiplet, bs-broad singlet.

sTCO-JF646: Synthesized according to the published procedure (Jana et al., 2023).

sTCO-Fluorescein: In dry tetrahydrofuran (THF) (3 mL), sTCO-CO_2H (10 mg, 0.06 mmol) (O'Brien et al., 2018), and N-methylmorpholine (10 µL, 0.09 mmol) were taken under nitrogen atmosphere and stirrer under ice cold condition. Isobutyl chloroformate (10 µL, 0.07 mmol) was added dropwise to the reaction mixture and stirrer for 5 minutes. After that, 6-aminofluorescein (24 mg, 0.07 mmol) in dry THF (1 mL) was added portion-wise and the reaction mixture was allowed to warm to room temperature and stirring was continued for another 3 hours. The solvent was evaporated, and the residue dissolved in ethyl acetate. The solution was washed with water and saturated sodium bicarbonate solution. The organic layer was dried over sodium sulfate (Na_2SO_4) and the product (16 mg, 0.032 mmol) was purified by silica gel column chromatography (10-15% methanol in dichloromethane). Yield- 53%. ^{1}H NMR (400MHz, CD_3OD) *δ* 7.91 (1H, d), 7.65 (1H, d), 7.06 (1H, d), 6.89 (1H, s), 6.84-6.82 (1H, m), 6.74-6.67 (1H, m), 6.65 (1H, s), 6.59-656 (1H, m), 6.23 (1H, d), 5.92-5.86 (1H, m), 5.27-5.20 (1H, m), 2.48 (1H, d), 2.39-2.25 (3H, m), 2.04-1.94 (2H, d), 1.37-1.32 (1H, m), 1.24 (1H, t), 1.07 (1H, t), 1.01 (1H, d), 0.84-0.75 (1H, m).

sTCO-sulfo-Cy5: In 1 mL of dry dimethylformamide (DMF), 5 mg of the sulfo-Cy5-amine (0.007 mmol) and 3.5 mg (0.01 mmol) of activated 4-nitrophenyl ester of sTCO (Jang et al., 2020) were added under nitrogen atmosphere. Followed by N,N-diisopropylethylamine (DIPEA) (10 µL, 3 equiv.) was added to the reaction mixture and allowed to stirrer at room temperature for 12 hours. After that, the solvent was concentrated onto silica gel under reduced pressure and the product

(4 mg, 0.004 mmol) was purified by silica gel column chromatography (20-30% methanol in dichloromethane). At the beginning of column run, added 50 mL of 50% ethyl acetate and hexane to remove the DMF solvent. Yield 57%. ^{1}H NMR (400MHz, CD_3OD) δ 8.31 (2H, t), 7.97 (1H, s), 7.89 (2H, d), 7.87 (1H, dd), 7.33 (2H, d), 6.67 (1H, t), 6.32 (2H, dd), 5.87-5.79 (1H, m), 5.13-5.06 (1H, m), 4.13 (2H, t), 3.88 (2H, d), 3.72 (2H, quin.), 3.64 (3H, s), 3.21 (2H, q), 3.16 (2H, t), 3.09 (2H, t), 2.86 (4H, d), 2.29 (1H, d), 2.23-2.17 (3H, m), 1.89-1.79 (2H, m), 1.60 (2H, t), 1.38 (6H, s), 1.36 (6H, s), 0.91-0.83 (2H, m), 0.59-0.42 (2H, m), 0.45-0.37 (1H, m).

In-gel fluorescence

HEK293T/17 cells were harvested 36-48 hours after transfection and treated with 1x SDS sample buffer (Invitrogen). Equal amounts of proteins were loaded into 3-8% Tris-acetate gradient gels and electrophoresed at 150 V for 1 hr. Fluorescence image of the gel was obtained with an Amersham ImageQuant 800 (Cytiva, Marlborough, MA). GFP fluorescence was collected with excitation at 460 nm and a 525/20 nm emission filter). The gel was subsequently stained with Quick Coomassie solution and destained with distilled water for each 2 hours before image acquisition.

Statistical analysis

Data are presented as mean ± SEM, *n* is the number of single cells. Student's *t* test was used to test the significant difference between two groups, with paired test performed as appropriate. $P < 0.05$ was regarded as significant.

Figure Legends

Figure 1 Using the PhyB/PIF system to activate PI3K with light

The OptoPI3K system reversibly activates PI3K to generate PI(3,4,5)P_3 at the PM. (A) Diagram of PI3K subunits and domains illustrating the regulatory p85 and catalytic p110 subunits. iSH2 domain in p85 subunit interacts with p110. Binding of NGF to TrkA receptor triggers the translocation of PI3K to the PM, phosphorylation of PI(4,5)P_2 to PI(3,4,5)P_3 and fusion of TRPV1-containing vesicles with the PM. (B,C) Schematic diagram for OptoPI3K system using PIF-YPF or PIF-iSH2-YFP. PhyB-mCherry is tethered to the PM using CAAX lipidation (magenta star). The iSH2 domain of p85 is fused to PIF so that translocation of PIF-iSH2-YFP, together with endogenous p110, to the PM promotes PI(3,4,5)P_3 synthesis upon 650 nm light. (D) Monitoring PIF-iSH2-YFP translocation to and from the PM with 650 nm and 750 nm light, respectively (top, yellow). Synthesis of PI(3,4,5)P_3 follows PIF-iSH2-YFP translocation to the PM, as indicated by the localization of the PI(3,4,5)P_3 probe Akt-PH-CFP (bottom, sky blue). F-11 cells transiently expressing PhyB-mCherry-CAAX, PIF-iSH2-YFP, and Akt-PH-CFP were illuminated with 750 nm or 650 nm light as indicated with the upper bar. Collected traces of PIF-iSH2-YFP and Akt-PH-CFP normalized to the initial baselines during the first episode of 750 nm illumination. The black line indicates the mean of the data and the colored envelope represents the standard error of the mean (n = 8). Because of the very low density of PI(3,4,5)P_3 present in the PM even in light- or NGF-stimulated cells (Auger et al., 1989), we used total internal reflection fluorescence (TIRF) microscopy to measure PI(3,4,5)P_3 density instead of confocal microscopy. TIRF illumination decreases exponentially with distance from the coverslip, selectively illuminating and exciting fluorophores within ~150 nm of the PM (Lakowicz, 2006; Mattheyses and Axelrod, 2006). (E) Scatter plot of PIF-iSH2-YFP and Akt-PH-CFP fluorescence for individual cells. Each point represents the 20 s average for 750 nm (2.66 - 3 min), 650 nm

(5.66 - 6 min), and 750 nm (8.66 - 9 min). Translocation of both PIF-iSH2-YFP and Akt-PH-CFP is reversible.

Figure 1 – figure supplement 1. PIF-YFP translocates to PM in response to 650 nm light and back to the cytosol in response to 750 nm light.

The PhyB –PIF light-inducible interaction is rapid (a few tens of seconds) and fully reversible (within ~30 seconds) and can be repeated multiple times. (A) Schematic diagram for optogenetic PhyB-PIF system. PhyB-mCherry loaded with the chromophore phycocyanobilin localizes to the PM due to a CAAX tag to induce lipidation (squiggly line). Illumination with 650 nm light induces a conformational change in PhyB that increases its affinity for PIF-YFP, effectively recruiting PIF-YFP to the PM. The conformational change in PhyB reverses with illumination with 750 nm light, causing PIF-YFP to dissociate and return to the cytoplasm. (B) A representative confocal experiment with an NIH3T3 cell stably expressing PhyB-mCherry-CAAX and PIF-YFP. Images were obtained at times indicated in C and are all shown on the same lookup table. During illumination with 650 nm light, PIF-YFP translocated to the PM quickly, with a corresponding decrease in cytoplasmic fluorescence. (C) Ratio of measured PIF fluorescence at region of interest (ROI) placed at the PM ($F_{Membrane}$) and cytoplasm ($F_{cytosol}$) from the cell in B. These data recapitulate previously published data (Levskaya et al., 2009; Toettcher et al., 2011).

Figure 1 – figure supplement 2. Detection of PI(3,4,5)P_3 generated by PIF-iSH2-YFP at the PM using GRP1-PH-CFP. (A) TIRF measurements of F-11 cells expressing PhyB-mCherry, PIF-iSH2-YFP, and GRP1-PH-CFP (n = 9). Upon 650 nm illumination, PIF PIF-iSH2-YFP translocated to the PM quickly (upper trace) while GRP1-PH-CFP moved slower (lower trace). Normalized to the initial 3 min control period. (B) Scatter plot of PIF-iSH2-YFP and GRP1-PH-CFP fluorescence for individual cells. Each point represents the 30 s average for 750 nm (2.5-3

min), 650 nm (7.5-8 min), and 750 nm (12.5-13 min). Translocation of both PIF-iSH2-YFP and GRP1-PH-CFP is reversible.

Figure 2. Activation of PI3K with light is sufficient to induce trafficking of TRPV1 to the PM.

Simultaneous TIRF measurement of PI(3,4,5)P_3 (cyan) and TRPV1 (yellow) in the PM in response to either (A) NGF or (C) light. (A) F-11 cells were transfected with TrkA/p75NTR, Akt-PH-CFP, and TRPV1-YFP. NGF (100 ng/mL) was applied during the times indicated by the bar/shading. Plotted are the PM-associated fluorescence in Akt-PH-CFP (top, cyan) and TRPV1-YFP (bottom, yellow) within the cell footprints. Data are reproduced from (Stratiievska et al., 2018) (C) F-11 cells transfected with PhyB-mCherry-CAAX, PIF-ISH2 (without a fluorescent tag), Akt-PH-CFP, and TRPV1-YFP were illuminated with 750 nm or 650 nm light as indicated. Color scheme as in (A), with line indicating the mean and envelope indicated the standard error of the mean (n = 13 for Akt-PH-CFP; n = 16 for TRPV1-YFP). Note the poor or irreversible increase of PM PI(3,4,5)P_3 in the PM. Inset cartoons depict the model for retention of iSH2 at the PM via binding to TRPV1. (B, D) Scatter plots of for individual cells. Each point represents the 20 s average for before (0.83 – 1.17 min) and after NGF (14.8 – 15.2 min) or for before (1.31 – 1.63 min) and after 650 nm (10.8 -11.2 min).

Figure 2 – figure supplement 1. 750 nm light fails to cause iSH2 dissociation from the PM in TRPV1-expressing cells.

(A) TIRF measurements of PIF-iSH2-YFP from F-11 cells expressing TRPV1-CFP in F-11 cells and HEK293T/17 cells, as indicated (n = 5 – 17). The color code and lines/envelopes have the same meaning as in Figure 2. Inset cartoons depict the model for retention of iSH2 at the PM via binding to TRPV1, which contains the PI3K-binding ARD domain. (B) Scatter plot of PIF-

iSH2-YFP fluorescence for individual cells. Each point represents the 20 s average for 750 nm (1.33 - 1.66 min), 650 nm (4.33 - 4.66 min), and 750 nm (7.33 - 7.66 min). Translocation of PIF-iSH2-YFP is irreversible. (C,D) The same experiments with continuous illumination at 750 nm (n = 5 – 13).

Figure 2 – figure supplement 2. PIF-YFP dissociates from the PM in response to 750 nm light even in TRPV1-expressing cells.

TRPV1 does not retain PIF lacking iSH2 at the PM of F-11 cells. (A) Normalized TIRF fluorescence was recorded in F-11 cells transfected with PhyB-mCherry-CAAX, PIF-YFP (no iSH2 domain), and either TRPV1-CFP or TRPV1 (no fluorescent tag). Reversible translocation of PIF-YFP upon 650 nm illumination demonstrates that PIF lacking iSH2 domain does not interact with TRPV1 channels on the PM (n = 8). (B) Scatter plot of PIF-iSH2-YFP fluorescence for individual cells. Each point represents the 20 s average for 750 nm (1.33 - 1.66 min), 650 nm (4.33 - 4.66 min), and 750 nm (7.33 - 7.66 min).

Figure 2 – figure supplement 3. 750 nm light succeeds in causing iSH2 dissociation from the PM in TRPM4-expressing cells.

(A) TIRF measurements of PIF-iSH2-YFP from F-11 and HEK293T/17 cells expressing TRPM4-CFP (n = 7 -17). Inset cartoons depict the model for no retention of iSH2 at the PM via binding to TRPM4, which has no ankyrin repeats. (B) Scatter plot of PIF-iSH2-YFP fluorescence for individual cells. Each point represents the 20 s average for 750 nm (1.33 - 1.66 min), 650 nm (4.33 - 4.66 min), and 750 nm (7.33 - 7.66 min).

Figure 3. Labeling the TRPV1 and InsR with membrane-impermeant sTCO-Cy5.

Confocal imaging illustrates the labeling of membrane proteins incorporating the ncAA Tet3-Bu with sTCO-sulfo-Cy5 in HEK293T/17 cells. The membrane impermeable dye labeled only the

proteins on the PM. (A) Schematic of the reaction between Tet3-Bu and sTCO-conjugated dyes. (B) Cartoon representing the selective labeling of membrane proteins incorporating Tet3-Bu at an extracellular site with membrane-impermeant sTCO-sulfo-Cy5. (C & E) Confocal images of HEK293T/17 cells expressing (C) TRPV1-468Tet3-Bu-GFP or (E) InsR-676Tet3-Bu-GFP. GFP fluorescence reflects expression of the proteins in the confocal volume across the field of view. Initially the cells did not show any detectable Cy5 fluorescence but after incubation of several minutes of 200 nM sTCO-sulfo-Cy5 showed Cy5 fluorescence at the PM. The Cy 5 images shown for (C) TRPV1-Tet3-Bu and (E) InsR-Tet3-Bu were obtained at the end of the experiment (20 minutes). (D & F) The graphs summarize the Cy5 fluorescence at the PM in (D) TRPV1-Tet3-Bu-GFP or (F) InsR-Tet3-Bu-GFP expressing cells. Solid traces represent the mean and envelopes the standard error of the mean (n = 3 for TRPV1 and n = 11 for InsR). Dashed traces represent a fit to the mean with a single exponential (tau = 17.8 minutes for TRPV1; tau = 13.8 minutes for InsR). Fits to the individual time courses for all the cells gave a mean of 18.2 minutes for TRPV1 (± 2.2 minutes) and 19.3 minutes for InsR (±4.0 minutes).

Figure 3– figure supplement 1. Incorporation of Tet3-Bu into TRPV1 and InsR.

(A) Whole-cell patch clamp recording demonstrates that TRPV1 incorporating Tet3-Bu remains functional. Application of 1 μM capsaicin to HEK-293T/17 cells transfected with either TRPV1-GFP (top) or TRPV1-468Tet3-Bu (bottom) induced inward currents at a holding potential of -60 mV. (B) Collected whole-cell electrophysiology data from all cells with peak capsaicin-activated currents normalized to the area of cell membrane (n = 8 and 9 for TRPV1-GFP and TRPV1-468Tet3-Bu, respectively). (C) In-gel fluorescence screening demonstrates that expression of full-length TRPV1-468Tet3-Bu or InsR-676Tet3-Bu requires the presence of Tet3-Bu ('Tet3-Bu (+)'). Wild type TRPV1-GFP is shown for reference. Detergent-extracted cell lysates were run on SDS/PAGE. GFP fluorescence (left) in the gels was measured and then cells were stained with Coomassie blue dye (right).

Figure 3– figure supplement 2. Activity of InsR-K676TAG measure as its recycling upon insulin treatment.

F-11 cells were transfected with the genetically modified receptor and inspected with a confocal microscope. (A) After labeling with membrane-impermeable sTCO-Cy3B dyes, the receptor was visible in the PM. Application of 100 nM insulin triggered the generation of endocytic granules (arrow heads). In some cells the receptor recycling was so vigorous that PM receptors nearly disappeared. (B) Scatter plot of the ratio of fluorescence between the cytoplasm and total cell area in individual cells (n = 12). (C) Structure of sTCO-Cy3B.

Figure 3– movie supplement 1. Activity of InsR-K676TAG measure as its recycling upon insulin treatment.

The same measurement as Figure 3– figure supplement 2A. Each image was obtained every 10 s. The time stamp is indicated on upper right corner and insulin application on upper left corner.

Figure 3 – figure supplement 3. Labelling of cells with sTCO conjugates of TAMRA, JF 646, fluorescein, and sulfo-Cy5.

HEK293T/17 cells expressing InsR-Tet3-Bu-GFP were labeled with sTCO dyes. For all dyes, shown are (left) confocal images of a representative field of HEK293T/17 cells incubated with the indicated concentration of sTCO-conjugated dye, (center) plots of the kinetics of cell labeling, and (right) diagrams of the fluorescent dyes. The confocal images were obtained ~30 s after washing off of extracellular dyes. GFP and bright field images are presented to demonstrate GFP-expressing (GFP(+)) and non-expressing (GFP(-)) cells. (A) 100 nM sTCO-

TAMRA; (B) 10 μM sTCO-JF 646; (C) 100 nM and 1 μM sTCO-fluorescein; and (D) 100 nM and 1 μM sTCO-sulfo-Cy5. For the plots, the intracellular fluorescence was normalized to the peak value at the end of the dye applications (A-C) or to the fluorescence from 1 μM extracellular sTCO-sulfo-Cy5 (D). The thick lines represent the mean of 6 - 9 cells for each dye, and the envelopes represent the standard errors of the mean.

Figure 4. Click chemistry labeling of TRPV1-468Tet3-Bu-GFP with sTCO-Cy5 to measure NGF-induced trafficking of TRPV1 to the PM.

HEK293T/17 cells expressing TRPV1-Tet3-Bu-GFP and NGF receptor were labeled with extracellular sTCO-sulfo-Cy5 and inspected with confocal microscopy. (A) Experimental protocol. Cells were incubated with 1 μM sTCO-sulfo-Cy5 for 5 min and free dye removed from the bath by washing for 2 minutes with dye-free Ringer's solution ('pulse-chase' labeling. F_0). Then the cells were treated with 100 ng/mL NGF for 10 min before the second sulfo-Cy5 labeling (F_1). Confocal images after initial sTCO-sulfo-Cy5 labeling (B) and after the 10 minute treatment with NGF and subsequent sTCO-sulfo-Cy5 labeling (C). (D) Summary scatter plot from multiple measurements, with individual experiments shown as dots and the mean of the experiments as black bars. The effect of NGF on GFP and sulfo-Cy5 signals is presented as a ratio of F_1/F_0 (n = 24). After NGF treatment, the ratio increased for sulfo-Cy5 significantly ($P < 0.001$) but not for GFP ($P = 0.64$). (E) The same experiment without NGF treatment ('Vehicle only', n = 5). Vehicle treatment did not change both GFP ($P = 0.63$) and sulfo-Cy5 ($P = 0.78$).

Figure 5. Measuring light-activated PI3K-induced TRPV1 and InsR trafficking to the PM using click chemistry

(A) Illustration of the experimental protocol. HEK293T/17 cells expressing TRPV1-468Tet3-Bu-GFP and InsR-676Tet3-Bu-GFP. (B) Confocal images sulfo-Cy5 obtained at different stages as depicted in (A). (C) Bright field (left) and confocal (middle and right) images obtained at the end of experiment. Comparison of bright-field (left) and GFP (middle) distinguishes TRPV1-Tet3-Bu-

GFP expressing cells from untransfected cells. PhyB-mCherry images (red) indicate that most TRPV1-positive cells expressed significant levels of the PhyB/PIF machinery for activating PI3K. (D and E) Summary scatter plots from multiple experiments, with individual cells shown as dots and the mean shows as black lines (n = 20). The effects of 750 and 650 nm illumination on sulfo-Cy5 (D) and GFP (E) are presented as ratios of fluorescence intensity after illumination with the indicated wavelength of illumination to the initial fluorescence. (F-I) The same experiment for InsR-676Tet3-Bu-GFP trafficking (n = 24).

Figure 5 – figure supplement 1. Control experiment for light-activated PI3K-induced TRPV1 and InsR trafficking to the PM.

The same experiment as Figure 5 without 650 nm illumination. The cells were exposed to 750 nm throughout the recording (n = 11 and 10 for TRPV1-Tet3-Bu-GFP and InsR-676Tet3-Bu-GFP, respectively)

Figure 6. Synthesis of sTCO-Fluorescein and sTCO-sulfo-Cy5.

Schemes illustrating the synthesis pathways for the indicated dyes.

Figure 6 – figure supplement 1. ^{1}H NMR spectra of synthesized compounds (A) sTCO-fluorescein and (B) sTCO-sulfo-Cy5.

Acknowledgements

Research reported in this publication was supported in part by the National Institute of General Medical Sciences of the National Institutes of Health under award numbers R35GM145225 (to SEG) and GCE4All Biomedical Technology Development and Dissemination Center RM1GM144227 (to RAM) and the following additional awards from the National Institutes of Health: S10RR025429, P30DK017047, and P30EY001730. This was also supported in part by

grants from the National Science Foundation NSF-2054824 (to RAM) and NSF-2129209 (to ENS). We thank Dr. Seung-Ryoung Jung for help with TIRF microscopy experiments.

References

Arsić, A., C. Hagemann, N. Stajković, T. Schubert, and I. Nikić-Spiegel. 2022. Minimal genetically encoded tags for fluorescent protein labeling in living neurons. *Nat Commun*. 13:314.

Auger, K.R., L.A. Serunian, S.P. Soltoff, P. Libby, and L.C. Cantley. 1989. PDGF-dependent tyrosine phosphorylation stimulates production of novel polyphosphoinositides in intact cells. *Cell*. 57:167-175.

Bae, C., C. Anselmi, J. Kalia, A. Jara-Oseguera, C.D. Schwieters, D. Krepkiy, C. Won Lee, E.H. Kim, J.I. Kim, J.D. Faraldo-Gómez, and K.J. Swartz. 2016. Structural insights into the mechanism of activation of the TRPV1 channel by a membrane-bound tarantula toxin. *Elife*. 5:e11273.

Bessa-Neto, D., G. Beliu, A. Kuhlemann, V. Pecoraro, S. Doose, N. Retailleau, N. Chevrier, D. Perrais, M. Sauer, and D. Choquet. 2021. Bioorthogonal labeling of transmembrane proteins with non-canonical amino acids unveils masked epitopes in live neurons. *Nat Commun*. 12:6715.

Bonini, S., L. Aloe, P. Rama, A. Lamagna, and A. Lambiase. 2002. Nerve growth factor (NGF): an important molecule for trophism and healing of the ocular surface. *Adv Exp Med Biol*. 506:531-537.

Bonnington, J.K., and P.A. McNaughton. 2003. Signalling pathways involved in the sensitisation of mouse nociceptive neurones by nerve growth factor. *J Physiol*. 551:433-446.

Braslavsky, S.E., W. Gartner, and K. Schaffner. 1997. Phytochrome photoconversion. *Plant, Cell & Environment*. 20:700-706.

Camprubi-Robles, M., R. Planells-Cases, and A. Ferrer-Montiel. 2009. Differential contribution of SNARE-dependent exocytosis to inflammatory potentiation of TRPV1 in nociceptors. *Faseb j*. 23:3722-3733.

Carpentier, J.L., J.P. Paccaud, P. Gorden, W.J. Rutter, and L. Orci. 1992. Insulin-induced surface redistribution regulates internalization of the insulin receptor and requires its autophosphorylation. *Proc Natl Acad Sci U S A*. 89:162-166.

Caterina, M.J., M.A. Schumacher, M. Tominaga, T.A. Rosen, J.D. Levine, and D. Julius. 1997. The capsaicin receptor: a heat-activated ion channel in the pain pathway. *Nature*. 389:816-824.

Chen, Y., L. Huang, X. Qi, and C. Chen. 2019. Insulin Receptor Trafficking: Consequences for Insulin Sensitivity and Diabetes. *Int J Mol Sci*. 20:5007.

Chin, J.W. 2014. Expanding and reprogramming the genetic code of cells and animals. *Annu Rev Biochem*. 83:379-408.

Ebadi, M., R.M. Bashir, M.L. Heidrick, F.M. Hamada, H.E. Refaey, A. Hamed, G. Helal, M.D. Baxi, D.R. Cerutis, and N.K. Lassi. 1997. Neurotrophins and their receptors in nerve injury and repair. *Neurochem Int*. 30:347-374.

Francel, P.C., K. Harris, M. Smith, M.C. Fishman, G. Dawson, and R.J. Miller. 1987. Neurochemical characteristics of a novel dorsal root ganglion X neuroblastoma hybrid cell line, F-11. *J Neurochem*. 48:1624-1631.

Freund-Michel, V., and N. Frossard. 2008. The nerve growth factor and its receptors in airway inflammatory diseases. *Pharmacol Ther*. 117:52-76.

Gallego-Sandín, S., A. Rodríguez-García, M.T. Alonso, and J. García-Sancho. 2009. The endoplasmic reticulum of dorsal root ganglion neurons contains functional TRPV1 channels. *J Biol Chem*. 284:32591-32601.

Geering, B., P.R. Cutillas, G. Nock, S.I. Gharbi, and B. Vanhaesebroeck. 2007. Class IA phosphoinositide 3-kinases are obligate p85-p110 heterodimers. *Proc Natl Acad Sci U S A*. 104:7809-7814.

Gregorio-Teruel, L., P. Valente, B. Liu, G. Fernández-Ballester, F. Qin, and A. Ferrer-Montiel. 2015. The Integrity of the TRP Domain Is Pivotal for Correct TRPV1 Channel Gating. *Biophys J*. 109:529-541.

Gregory, K.J., R. Velagaleti, D.M. Thal, R.M. Brady, A. Christopoulos, P.J. Conn, and D.J. Lapinsky. 2016. Clickable Photoaffinity Ligands for Metabotropic Glutamate Receptor 5 Based on Select Acetylenic Negative Allosteric Modulators. *ACS Chem Biol*. 11:1870-1879.

Hamill, O.P., A. Marty, E. Neher, B. Sakmann, and F.J. Sigworth. 1981. Improved patch-clamp techniques for high-resolution current recording from cells and cell-free membrane patches. *Pflugers Arch*. 391:85-100.

Hawkins, P.T., K.E. Anderson, K. Davidson, and L.R. Stephens. 2006. Signalling through Class I PI3Ks in mammalian cells. *Biochem Soc Trans*. 34:647-662.

Hawkins, P.T., and L.R. Stephens. 2015. PI3K signalling in inflammation. *Biochim Biophys Acta*. 1851:882-897.

Hoffmann, J.E., T. Plass, I. Nikić, I.V. Aramburu, C. Koehler, H. Gillandt, E.A. Lemke, and C. Schultz. 2015. Highly Stable trans-Cyclooctene Amino Acids for Live-Cell Labeling. *Chemistry*. 21:12266-12270.

Idevall-Hagren, O., E.J. Dickson, B. Hille, D.K. Toomre, and P. De Camilli. 2012. Optogenetic control of phosphoinositide metabolism. *Proc Natl Acad Sci U S A*. 109:E2316-2323.

Iraburu, M.J., T. Garner, and C. Montiel-Duarte. 2021. Revising Endosomal Trafficking under Insulin Receptor Activation. *Int J Mol Sci*. 22:6978.

Jana, S., E.G.B. Evans, H.S. Jang, S. Zhang, H. Zhang, A. Rajca, S.E. Gordon, W.N. Zagotta, S. Stoll, and R.A. Mehl. 2023. Ultrafast Bioorthogonal Spin-Labeling and Distance Measurements in Mammalian Cells Using Small, Genetically Encoded Tetrazine Amino Acids. *J Am Chem Soc*. 145:14608-14620.

Jang, H.S., S. Jana, R.J. Blizzard, J.C. Meeuwsen, and R.A. Mehl. 2020. Access to Faster Eukaryotic Cell Labeling with Encoded Tetrazine Amino Acids. *J Am Chem Soc*. 142:7245-7249.

Jara-Oseguera, A., C. Bae, and K.J. Swartz. 2016. An external sodium ion binding site controls allosteric gating in TRPV1 channels. *Elife*. 5:13356.

Jeske, N.A., A. Diogenes, N.B. Ruparel, J.C. Fehrenbacher, M. Henry, A.N. Akopian, and K.M. Hargreaves. 2008. A-kinase anchoring protein mediates TRPV1 thermal hyperalgesia through PKA phosphorylation of TRPV1. *Pain*. 138:604-616.

Jeske, N.A., A.M. Patwardhan, N.B. Ruparel, A.N. Akopian, M.S. Shapiro, and M.A. Henry. 2009. A-kinase anchoring protein 150 controls protein kinase C-mediated phosphorylation and sensitization of TRPV1. *Pain*. 146:301-307.

Jones, C.M., D.M. Robkis, R.J. Blizzard, M. Munari, Y. Venkatesh, T.S. Mihaila, A.J. Eddins, R.A. Mehl, W.N. Zagotta, S.E. Gordon, and E.J. Petersson. 2021. Genetic encoding of a highly photostable, long lifetime fluorescent amino acid for imaging in mammalian cells. *Chem Sci*. 12:11955-11964.

Katrin Anders, L.-O.E. 2015. The family of phytochrome-like photoreceptors: diverse, complex and multi-colored, but very useful. 35:7–16.

Keller, M., S.A. Mahuroof, V. Hong Yee, J. Carpenter, L. Schindler, T. Littmann, A. Pegoli, H. Hübner, G. Bernhardt, P. Gmeiner, and N.D. Holliday. 2020. Fluorescence Labeling of Neurotensin(8-13) via Arginine Residues Gives Molecular Tools with High Receptor Affinity. *ACS Med Chem Lett*. 11:16-22.

Kenry, and B. Liu. 2019. Bio-orthogonal Click Chemistry for In Vivo Bioimaging. *Trends in Chemistry*. 1:763-778.

Klippel, A., J.A. Escobedo, Q. Hu, and L.T. Williams. 1993. A region of the 85-kilodalton (kDa) subunit of phosphatidylinositol 3-kinase binds the 110-kDa catalytic subunit in vivo. *Mol Cell Biol*. 13:5560-5566.

Knutson, V.P. 1991. Cellular trafficking and processing of the insulin receptor. *FASEB J*. 5:2130-2138.

Koh, D.S., L. Chen, C.A. Ufret-Vincenty, and S.R. Jung. 2011. A fast solution switching system with temperature control for single cell measurements. *J Neurosci Methods*. 199:35-42.

Koh, D.S., and B. Hille. 1997. Modulation by neurotransmitters of catecholamine secretion from sympathetic ganglion neurons detected by amperometry. *Proc Natl Acad Sci U S A*. 94:1506-1511.

Kozma, E., I. Nikić, B.R. Varga, I.V. Aramburu, J.H. Kang, O.T. Fackler, E.A. Lemke, and P. Kele. 2016. Hydrophilic trans-Cyclooctenylated Noncanonical Amino Acids for Fast Intracellular Protein Labeling. *ChemBioChem*. 17:1518-1524.

Kuhlemann, A., G. Beliu, D. Janzen, E.M. Petrini, D. Taban, D.A. Helmerich, S. Doose, M. Bruno, A. Barberis, C. Villmann, M. Sauer, and C. Werner. 2021. Genetic Code Expansion and Click-Chemistry Labeling to Visualize GABA-A Receptors by Super-Resolution Microscopy. *Front Synaptic Neurosci*. 13:727406.

Lakowicz, J.R. 2006. Principles of fluorescence spectroscopy. 3rd.ed. Springer, New York. xxvi, 954 pages pp.

Lam, R., A.B. Gondin, M. Canals, B. Kellam, S.J. Briddon, B. Graham, and P.J. Scammells. 2018. Fluorescently Labeled Morphine Derivatives for Bioimaging Studies. *J Med Chem*. 61:1316-1329.

Lambiase, A., L. Manni, S. Bonini, P. Rama, A. Micera, and L. Aloe. 2000. Nerve growth factor promotes corneal healing: structural, biochemical, and molecular analyses of rat and human corneas. *Invest Ophthalmol Vis Sci*. 41:1063-1069.

Lang, K., and J.W. Chin. 2014. Bioorthogonal reactions for labeling proteins. *ACS Chem Biol*. 9:16-20.

Lemmon, M. 2008. Membrane recognition by phospholipid-binding domains. *Nat Rev Mol Cell Biol*. 9:99-111.

Lemmon, M.A., and J. Schlessinger. 2010. Cell signaling by receptor tyrosine kinases. *Cell*. 141:1117-1134.

Levskaya, A., O.D. Weiner, W.A. Lim, and C.A. Voigt. 2009. Spatiotemporal control of cell signalling using a light-switchable protein interaction. *Nature*. 461:997-1001.

Liu, M., M.C. Liu, C. Magoulas, J.V. Priestley, and N.J. Willmott. 2003. Versatile regulation of cytosolic Ca2+ by vanilloid receptor I in rat dorsal root ganglion neurons. *J Biol Chem*. 278:5462-5472.

Ma, L., F. Yang, S. Vu, and J. Zheng. 2016. Exploring functional roles of TRPV1 intracellular domains with unstructured peptide-insertion screening. *Sci Rep*. 6:33827.

Mateos-Gil, P., S. Letschert, S. Doose, and M. Sauer. 2016. Super-Resolution Imaging of Plasma Membrane Proteins with Click Chemistry. *Front Cell Dev Biol*. 4:98.

Mathivanan, S., I. Devesa, J.P. Changeux, and A. Ferrer-Montiel. 2016. Bradykinin Induces TRPV1 Exocytotic Recruitment in Peptidergic Nociceptors. *Front Pharmacol*. 7:178.

Mattheyses, A.L., and D. Axelrod. 2006. Direct measurement of the evanescent field profile produced by objective-based total internal reflection fluorescence. *J Biomed Opt*. 11:014006.

McMahan, S., M. Koltzenburg, I. Tracey, and D. Turk. 2013. Wall and Melzack's Textbook of Pain. 6th Edition.ed. Elsevier Saunders.

Meijer, A., S. Otto, and J.B.F.N. Engberts. 1998. Effects of the Hydrophobicity of the Reactants on Diels-Alder Reactions in Water. *Journal of Organic Chemistry*. 63:8989-8994.

Meineke, B., J. Heimgärtner, J. Eirich, M. Landreh, and S.J. Elsässer. 2020. Site-Specific Incorporation of Two ncAAs for Two-Color Bioorthogonal Labeling and Crosslinking of Proteins on Live Mammalian Cells. *Cell Rep*. 31:107811.

Meng, J., J. Wang, M. Steinhoff, and J.O. Dolly. 2016. TNFα induces co-trafficking of TRPV1/TRPA1 in VAMP1-containing vesicles to the plasmalemma via Munc18–1/syntaxin1/SNAP-25 mediated fusion. *Scientific Reports*. 6:21226.

Montecinos-Franjola, F., B.L. Bauer, J.A. Mears, and R. Ramachandran. 2020. GFP fluorescence tagging alters dynamin-related protein 1 oligomerization dynamics and creates disassembly-refractory puncta to mediate mitochondrial fission. *Sci Rep*. 10:14777.

Morenilla-Palao, C., R. Planells-Cases, N. Garcia-Sanz, and A. Ferrer-Montiel. 2004. Regulated exocytosis contributes to protein kinase C potentiation of vanilloid receptor activity. *J Biol Chem*. 279:25665-25672.

Murrey, H.E., J.C. Judkins, C.W. Am Ende, T.E. Ballard, Y. Fang, K. Riccardi, L. Di, E.R. Guilmette, J.W. Schwartz, J.M. Fox, and D.S. Johnson. 2015. Systematic Evaluation of Bioorthogonal Reactions in Live Cells with Clickable HaloTag Ligands: Implications for Intracellular Imaging. *J Am Chem Soc*. 137:11461-11475.

Nakazawa, Y., R.S. Petrova, Y. Sugiyama, N. Nagai, H. Tamura, and P.J. Donaldson. 2021. Regulation of the Membrane Trafficking of the Mechanosensitive Ion Channels TRPV1 and TRPV4 by Zonular Tension, Osmotic Stress and Activators in the Mouse Lens. *Int J Mol Sci*. 22:12658.

Neubert, F., G. Beliu, U. Terpitz, C. Werner, C. Geis, M. Sauer, and S. Doose. 2018. Bioorthogonal Click Chemistry Enables Site-specific Fluorescence Labeling of Functional NMDA Receptors for Super-Resolution Imaging. *Angew Chem Int Ed Engl*. 57:16364-16369.

Nichols, J.M., D. Veltman, and R.R. Kay. 2015. Chemotaxis of a model organism: progress with Dictyostelium. *Curr Opin Cell Biol*. 36:7-12.

Nikić, I., J.H. Kang, G.E. Girona, I.V. Aramburu, and E.A. Lemke. 2015. Labeling proteins on live mammalian cells using click chemistry. *Nat Protoc*. 10:780-791.

O'Brien, J.G.K., S.R. Chintala, and J.M. Fox. 2018. Stereoselective Synthesis of Bicyclo[6.1.0]nonene Precursors of the Bioorthogonal Reagents s-TCO and BCN. *J Org Chem*. 83:7500-7503.

Ojima, K., K. Shiraiwa, K. Soga, T. Doura, M. Takato, K. Komatsu, M. Yuzaki, I. Hamachi, and S. Kiyonaka. 2021. Ligand-directed two-step labeling to quantify neuronal glutamate receptor trafficking. *Nat Commun*. 12:831.

Peng, T., and H.C. Hang. 2016. Site-Specific Bioorthogonal Labeling for Fluorescence Imaging of Intracellular Proteins in Living Cells. *J Am Chem Soc*. 138:14423-14433.

Rasband, W.S. 1997. ImageJ. *In*. U. S. National Institutes of Health, Bethesda, Maryland, USA.

Reis, C., S. Chambel, A. Ferreira, and C.D. Cruz. 2022. Involvement of nerve growth factor (NGF) in chronic neuropathic pain - a systematic review. *Rev Neurosci*. 34:75-84.

Robinson, D.R., Y.M. Wu, and S.F. Lin. 2000. The protein tyrosine kinase family of the human genome. *Oncogene*. 19:5548-5557.

Row, R.D., and J.A. Prescher. 2018. Constructing New Bioorthogonal Reagents and Reactions. *Acc Chem Res*. 51:1073-1081.

Ryan, A., O. Shade, A. Bardhan, A. Bartnik, and A. Deiters. 2022. Quantitative Analysis and Optimization of Site-Specific Protein Bioconjugation in Mammalian Cells. *Bioconjug Chem*. 33:2361-2369.

Saltiel, A.R. 2021. Insulin signaling in health and disease. *J Clin Invest*. 131:e142241.

Sasaoka, T., T. Wada, H. Ishihara, Y. Takata, T. Haruta, I. Usui, M. Ishiki, and M. Kobayashi. 1999. Synergistic role of the phosphatidylinositol 3-kinase and mitogen-activated protein kinase cascade in the regulation of insulin receptor trafficking. *Endocrinology*. 140:3826-3834.

Schmied, W.H., S.J. Elsässer, C. Uttamapinant, and J.W. Chin. 2014. Efficient multisite unnatural amino acid incorporation in mammalian cells via optimized pyrrolysyl tRNA synthetase/tRNA expression and engineered eRF1. *J Am Chem Soc*. 136:15577-15583.

Schneider, C.A., W.S. Rasband, and K.W. Eliceiri. 2012. NIH Image to ImageJ: 25 years of image analysis. *Nat Methods*. 9:671-675.

Stein, A.T., C.A. Ufret-Vincenty, L. Hua, L.F. Santana, and S.E. Gordon. 2006. Phosphoinositide 3-Kinase Binds to TRPV1 and Mediates NGF-stimulated TRPV1 Trafficking to the Plasma Membrane. *J Gen Physiol*. 128:509-522.

Stratiievska, A., S. Nelson, E.N. Senning, J.D. Lautz, S.E. Smith, and S.E. Gordon. 2018. Reciprocal regulation among TRPV1 channels and phosphoinositide 3-kinase in response to nerve growth factor. *Elife*. 7:e38869.

Suh, B.C., T. Inoue, T. Meyer, and B. Hille. 2006. Rapid chemically induced changes of PtdIns(4,5)P2 gate KCNQ ion channels. *Science*. 314:1454-1457.

Taylor, M.T., M.L. Blackman, O. Dmitrenko, and J.M. Fox. 2011. Design and synthesis of highly reactive dienophiles for the tetrazine-trans-cyclooctene ligation. *J Am Chem Soc*. 133:9646-9649.

Thorpe, L.M., H. Yuzugullu, and J.J. Zhao. 2015. PI3K in cancer: divergent roles of isoforms, modes of activation and therapeutic targeting. *Nat Rev Cancer*. 15:7-24.

Toettcher, J.E., D. Gong, W.A. Lim, and O.D. Weiner. 2011. Light-based feedback for controlling intracellular signaling dynamics. *Nat Methods*. 8:837-839.

Tominaga, M., M.J. Caterina, A.B. Malmberg, T.A. Rosen, H. Gilbert, K. Skinner, B.E. Raumann, A.I. Basbaum, and D. Julius. 1998. The cloned capsaicin receptor integrates multiple pain-producing stimuli. *Neuron*. 21:531-543.

Tsien, R.Y. 1998. The green fluorescent protein. *Annu Rev Biochem*. 67:509-544.

Uda, Y., Y. Goto, S. Oda, T. Kohchi, M. Matsuda, and K. Aoki. 2017. Efficient synthesis of phycocyanobilin in mammalian cells for optogenetic control of cell signaling. *Proc Natl Acad Sci U S A*. 114:11962-11967.

Uda, Y., H. Miura, Y. Goto, K. Yamamoto, Y. Mii, Y. Kondo, S. Takada, and K. Aoki. 2020. Improvement of Phycocyanobilin Synthesis for Genetically Encoded Phytochrome-Based Optogenetics. *ACS Chem Biol*. 15:2896-2906.

Uttamapinant, C., J.D. Howe, K. Lang, V. Beránek, L. Davis, M. Mahesh, N.P. Barry, and J.W. Chin. 2015. Genetic code expansion enables live-cell and super-resolution imaging of site-specifically labeled cellular proteins. *J Am Chem Soc*. 137:4602-4605.

Xing, B.M., Y.R. Yang, J.X. Du, H.J. Chen, C. Qi, Z.H. Huang, Y. Zhang, and Y. Wang. 2012. Cyclin-dependent kinase 5 controls TRPV1 membrane trafficking and the heat sensitivity of nociceptors through KIF13B. *J Neurosci*. 32:14709-14721.

Yang, S., F. Yang, N. Wei, J. Hong, B. Li, L. Luo, M. Rong, V. Yarov-Yarovoy, J. Zheng, K. Wang, and R. Lai. 2015. A pain-inducing centipede toxin targets the heat activation machinery of nociceptor TRPV1. *Nat Commun*. 6:8297.

Ye, L., S. Maji, N. Sanghera, P. Gopalasingam, E. Gorbunov, S. Tarasov, O. Epstein, and J. Klein-Seetharaman. 2017. Structure and dynamics of the insulin receptor: implications for receptor activation and drug discovery. *Drug Discov Today*. 22:1092-1102.

Zhang, M., H. Jang, and R. Nussinov. 2020. Structural Features that Distinguish Inactive and Active PI3K Lipid Kinases. *J Mol Biol*. 432:5849-5859.

Zhang, X., J. Huang, and P.A. McNaughton. 2005. NGF rapidly increases membrane expression of TRPV1 heat-gated ion channels. *EMBO J*. 24:4211-4223.

Zhu, W., and G.S. Oxford. 2007. Phosphoinositide-3-kinase and mitogen activated protein kinase signaling pathways mediate acute NGF sensitization of TRPV1. *Mol Cell Neurosci*. 34:689-700.

Ziemba, B.P., J.E. Burke, G. Masson, R.L. Williams, and J.J. Falke. 2016. Regulation of PI3K by PKC and MARCKS: Single-Molecule Analysis of a Reconstituted Signaling Pathway. *Biophys J*. 110:1811-1825.

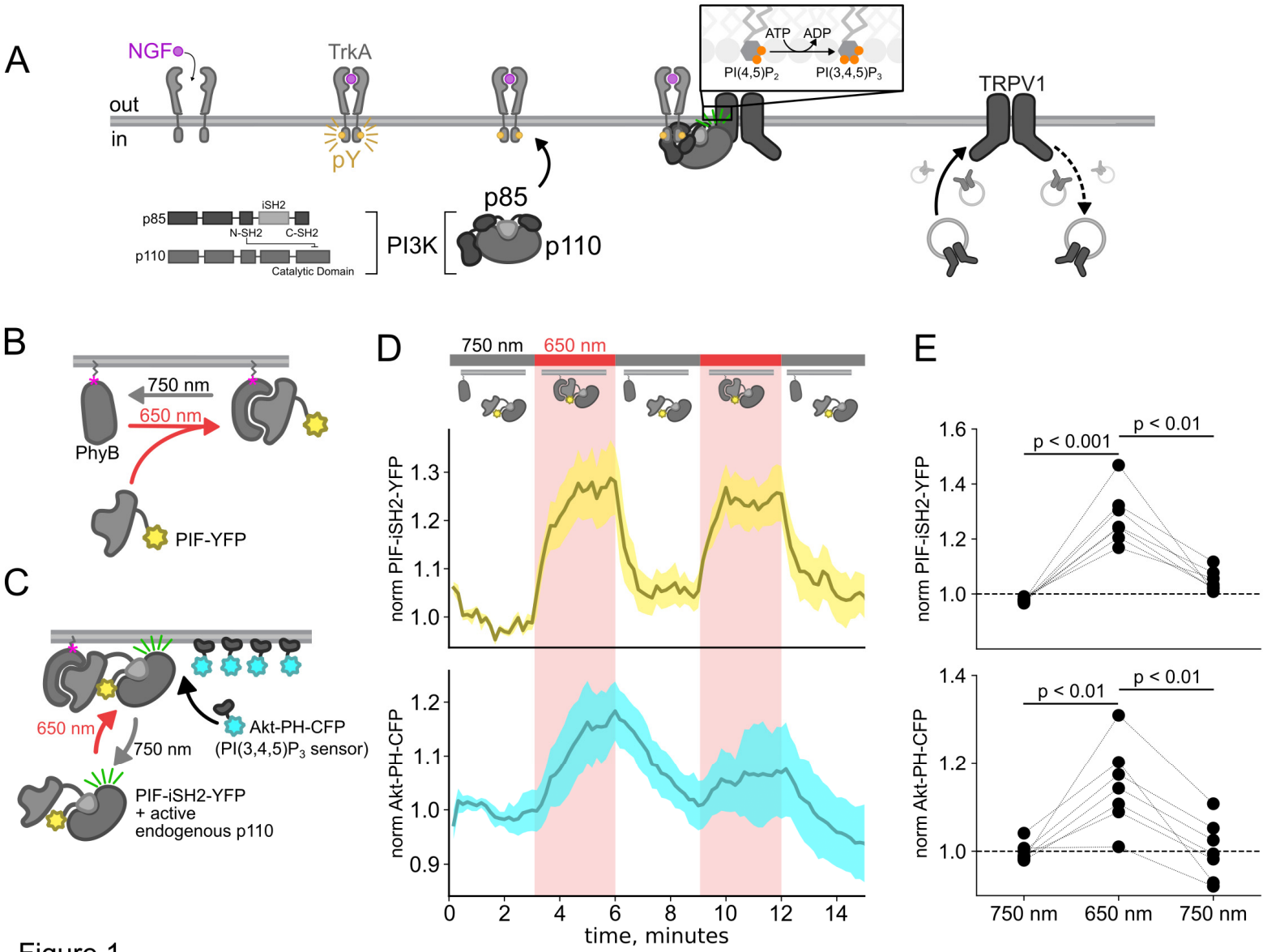
A
NGF
TrkA
out
in
pY
ATP
ADP
PI(4,5)P2
PI(3,4,5)P3
TRPV1
p85
iSH2
N-SH2
C-SH2
p110
Catalytic Domain
PI3K
p110
B
750 nm
650 nm
PhyB
PIF-YFP
C
650 nm
750 nm
Akt-PH-CFP
(PI(3,4,5)P3 sensor)
PIF-iSH2-YFP
+ active
endogenous p110
D
750 nm
650 nm
norm PIF-iSH2-YFP
norm Akt-PH-CFP
time, minutes
E
p < 0.001
p < 0.01
p < 0.01
p < 0.01
norm PIF-iSH2-YFP
norm Akt-PH-CFP
750 nm
650 nm
750 nm

Figure 1

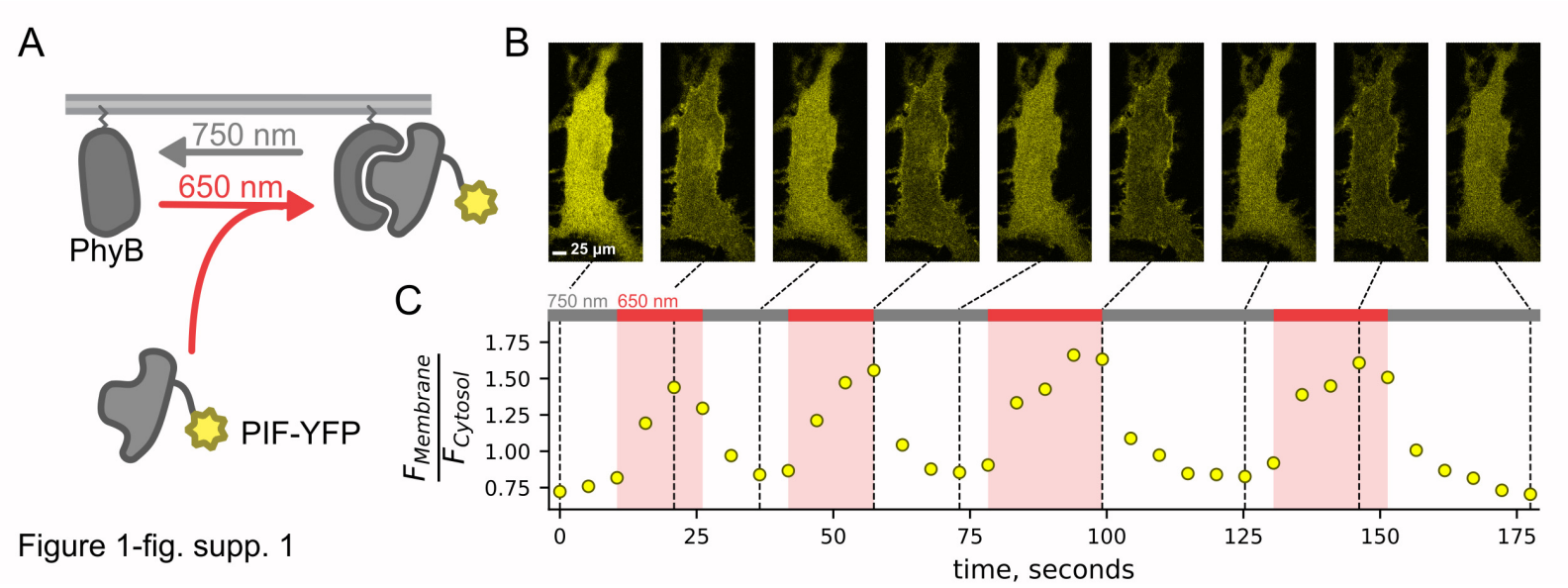

Figure 1-fig. supp. 1

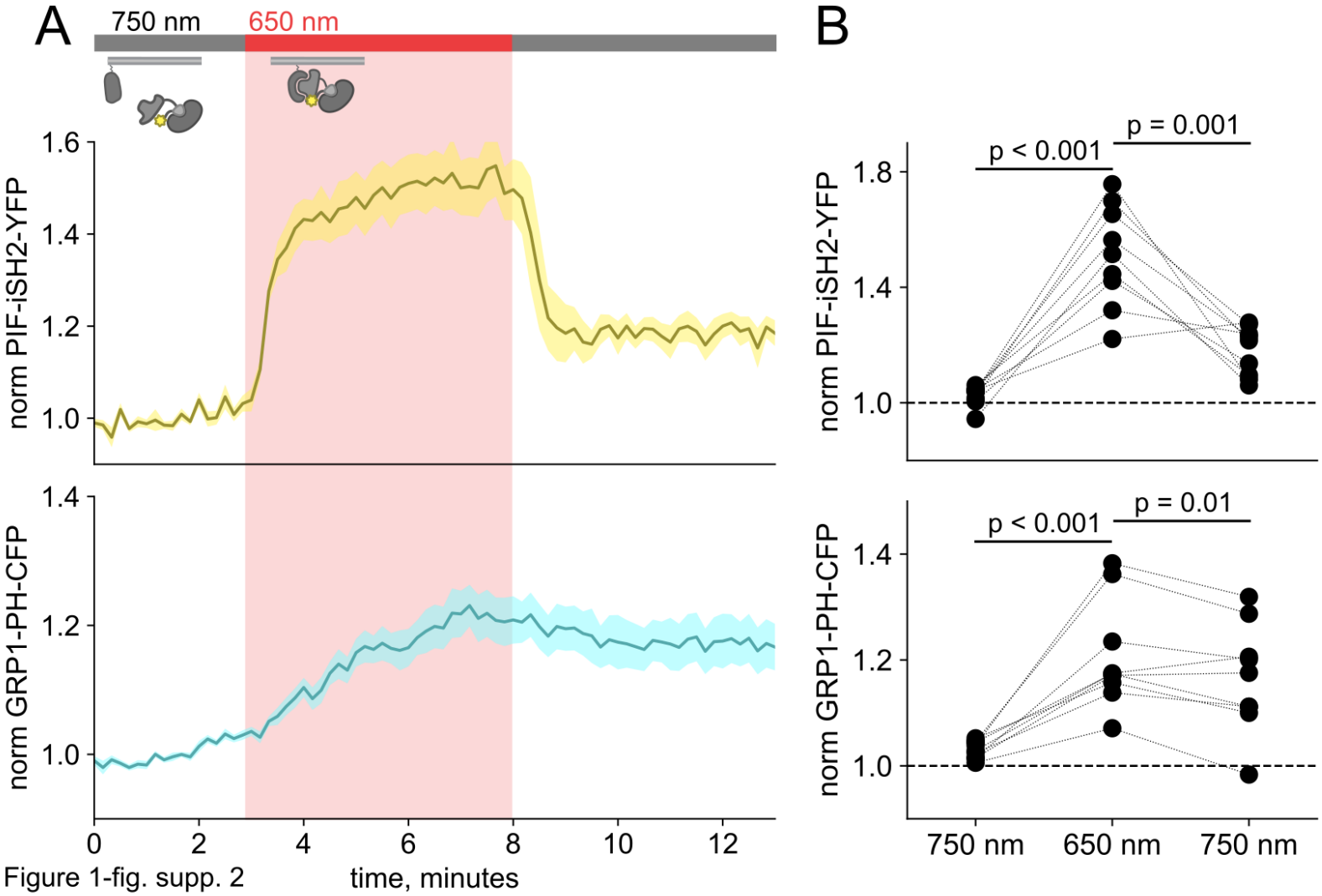

Figure 1-fig. supp. 2

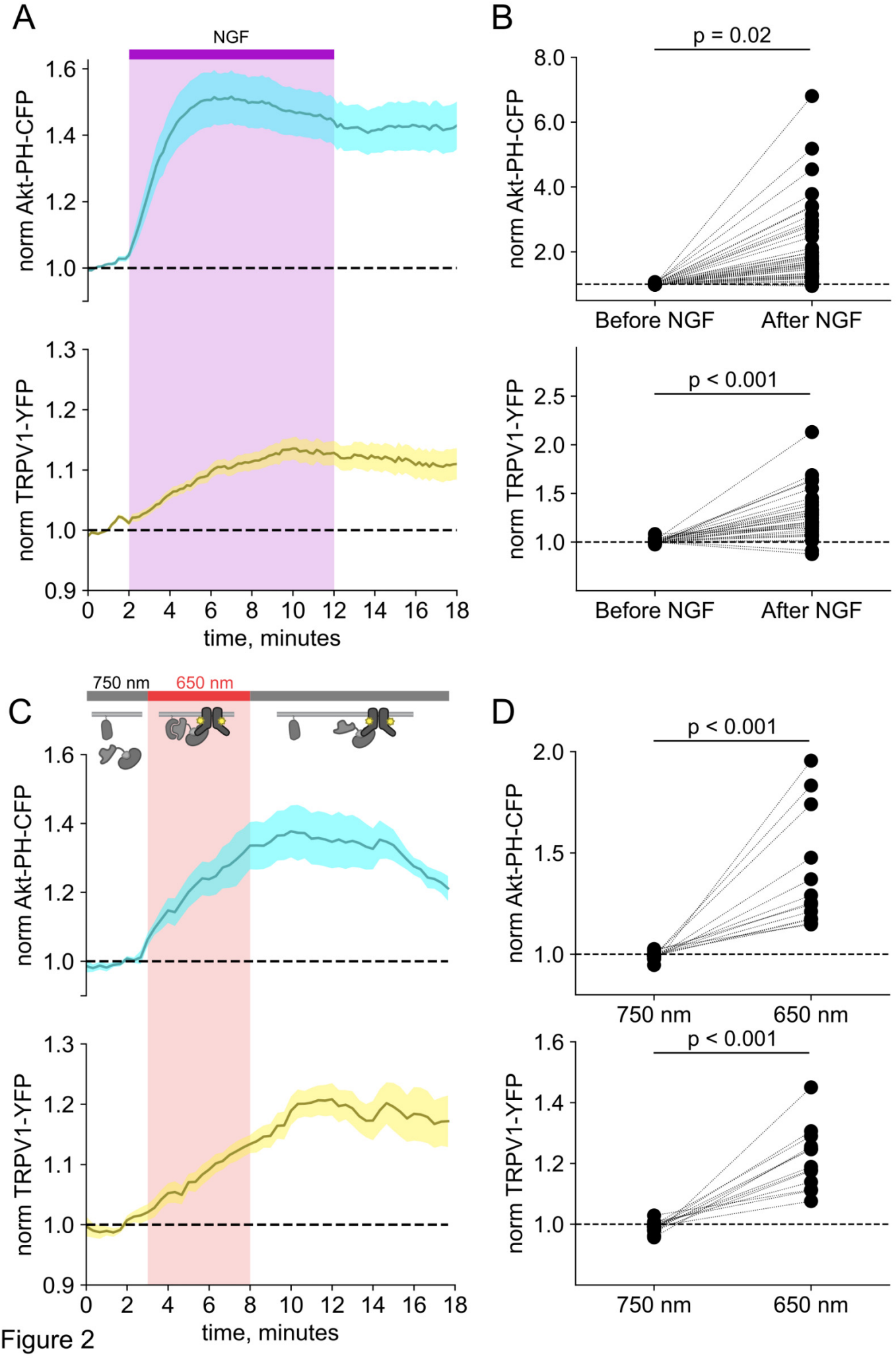
A
NGF
norm Akt-PH-CFP
norm TRPV1-YFP
time, minutes
B
p = 0.02
Before NGF
After NGF
p < 0.001
C
750 nm
650 nm
D
p < 0.001
750 nm
650 nm

Figure 2

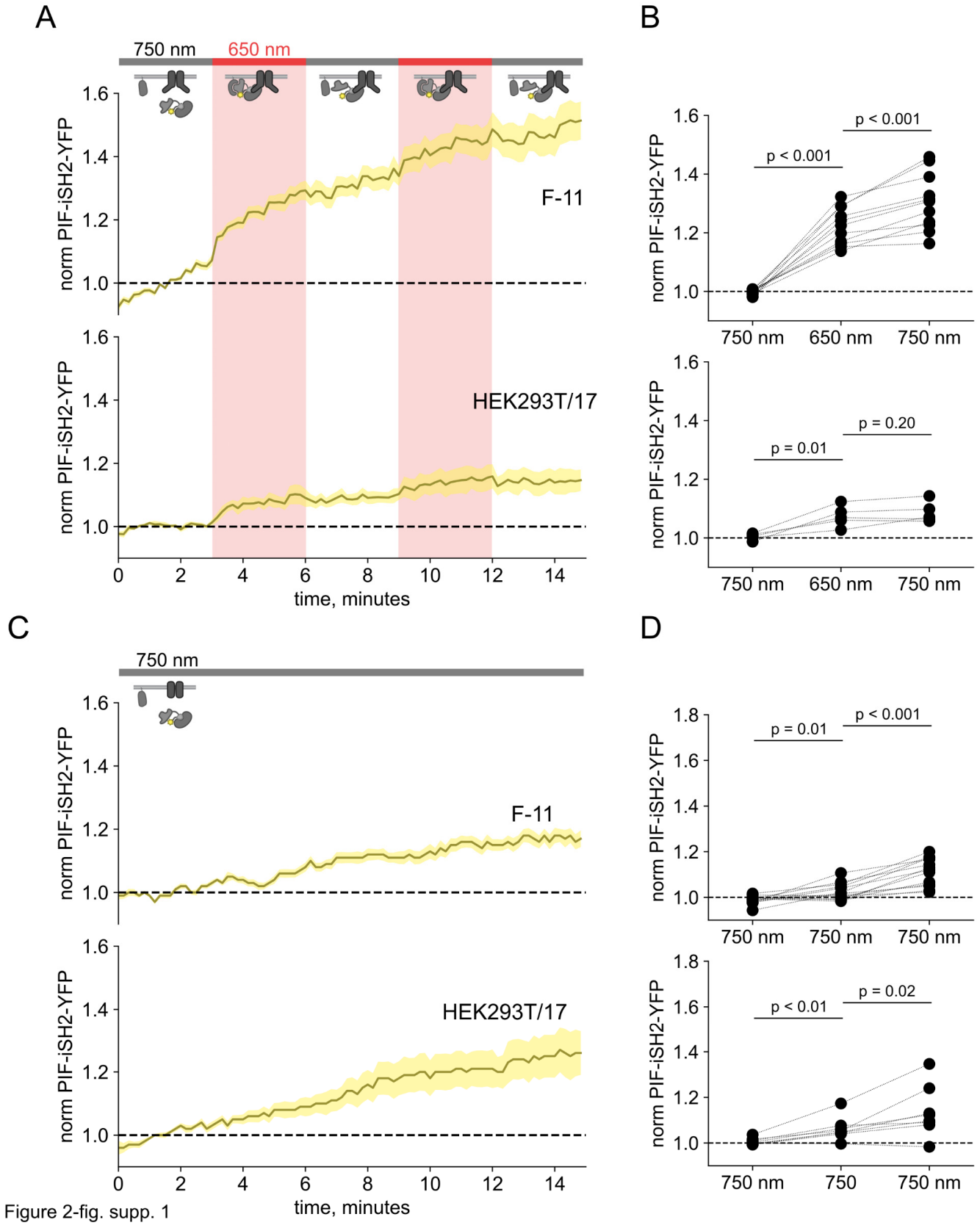

Figure 2-fig. supp. 1

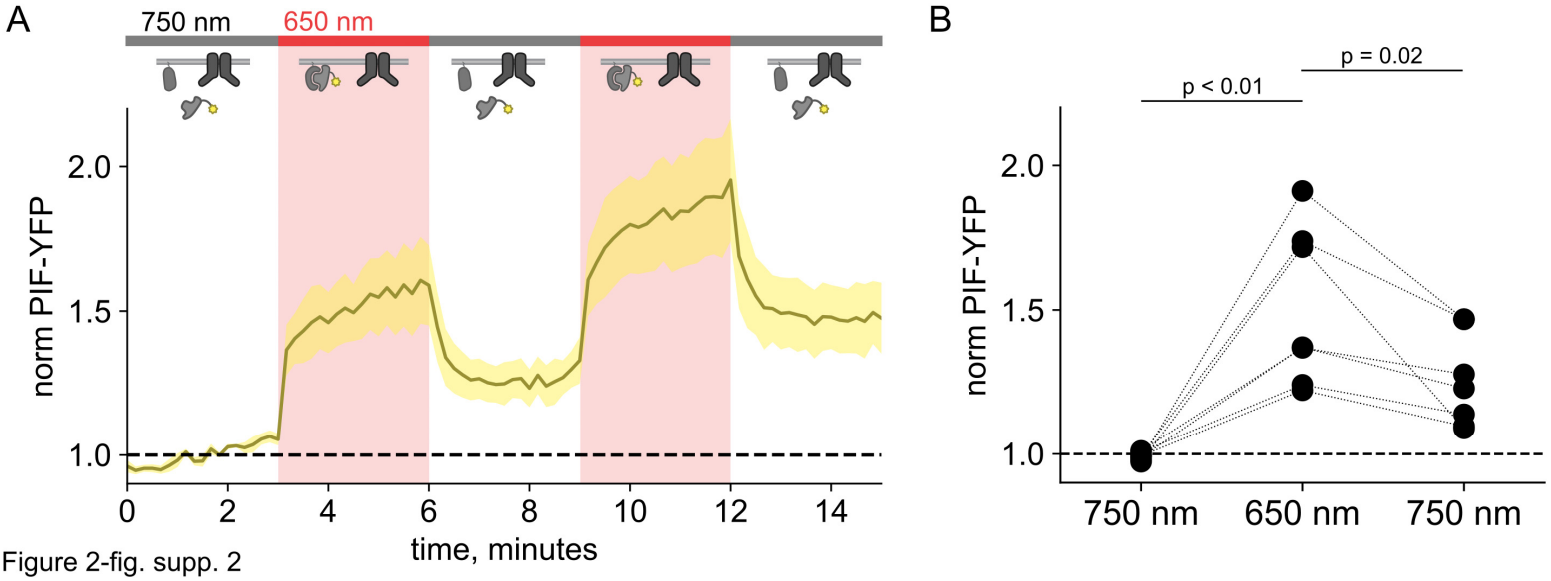

Figure 2-fig. supp. 2

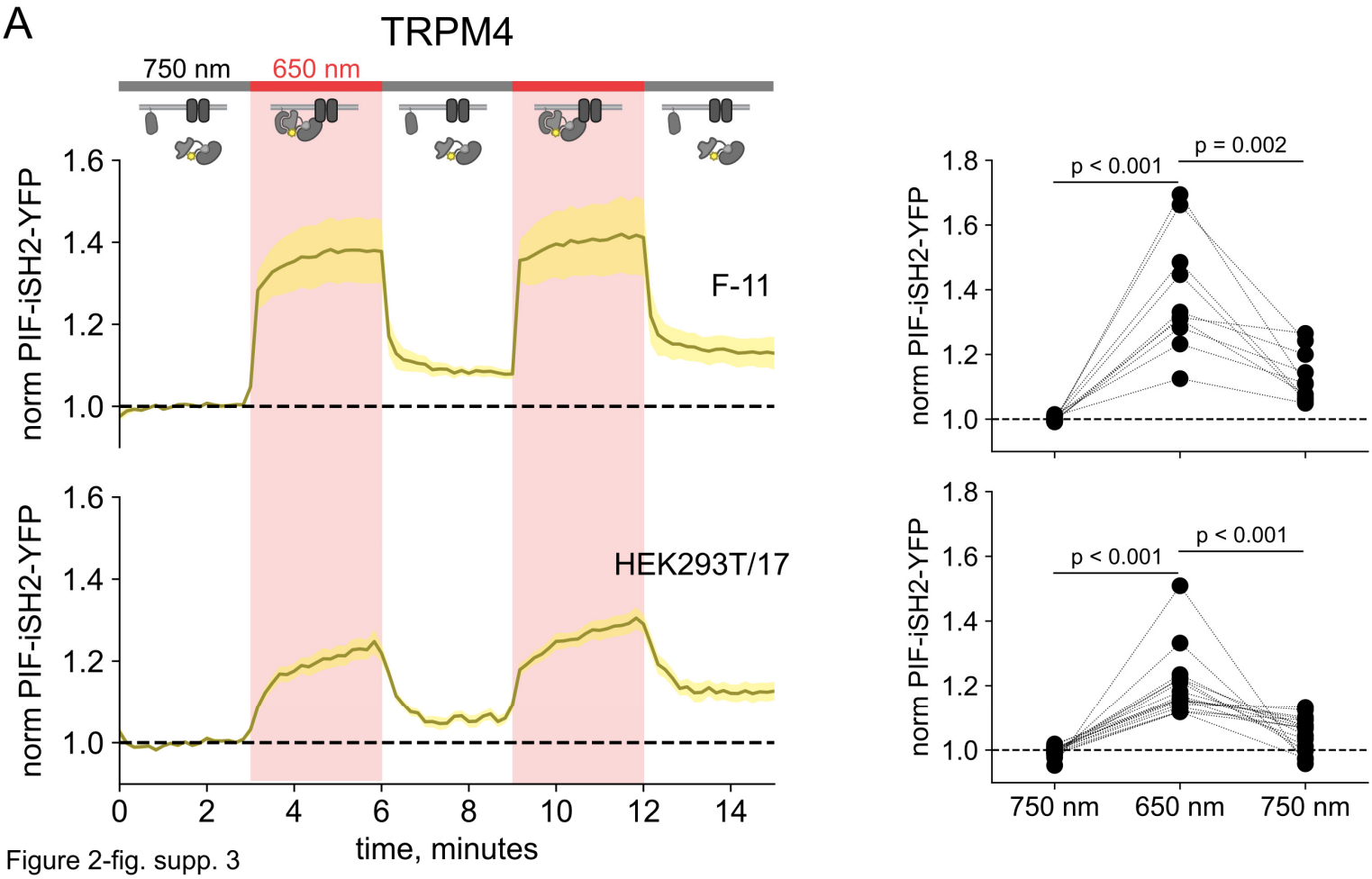

Figure 2-fig. supp. 3

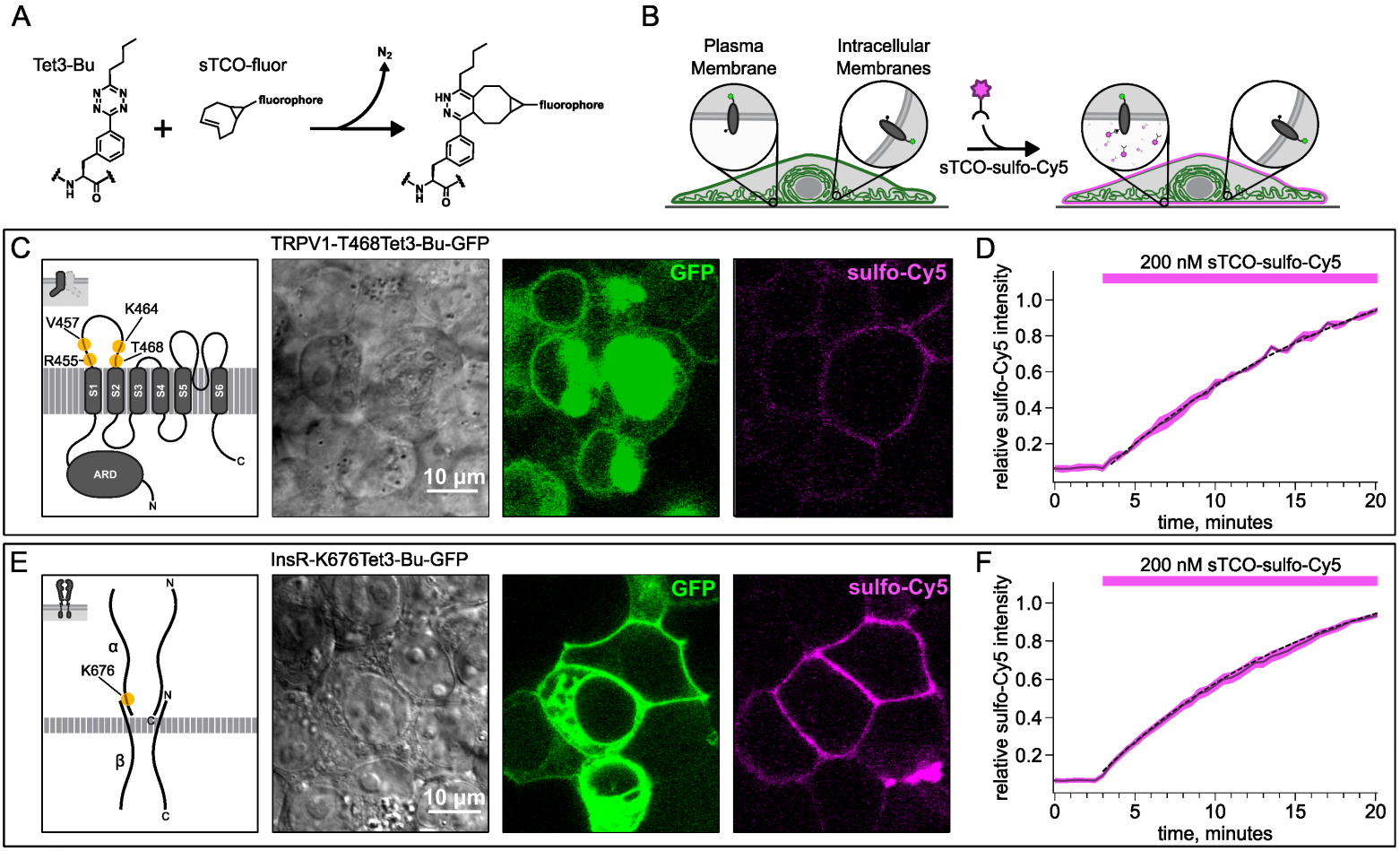
A
Tet3-Bu
sTCO-fluor
fluorophore
N2
fluorophore
B
Plasma Membrane
Intracellular Membranes
sTCO-sulfo-Cy5
C
TRPV1-T468Tet3-Bu-GFP
K464
V457
T468
R455
S1
S2
S3
S4
S5
S6
ARD
N
C
10 µm
GFP
sulfo-Cy5
D
200 nM sTCO-sulfo-Cy5
relative sulfo-Cy5 intensity
time, minutes
E
InsR-K676Tet3-Bu-GFP
α
K676
β
N
C
10 µm
GFP
sulfo-Cy5
F
200 nM sTCO-sulfo-Cy5
relative sulfo-Cy5 intensity
time, minutes

Figure 3

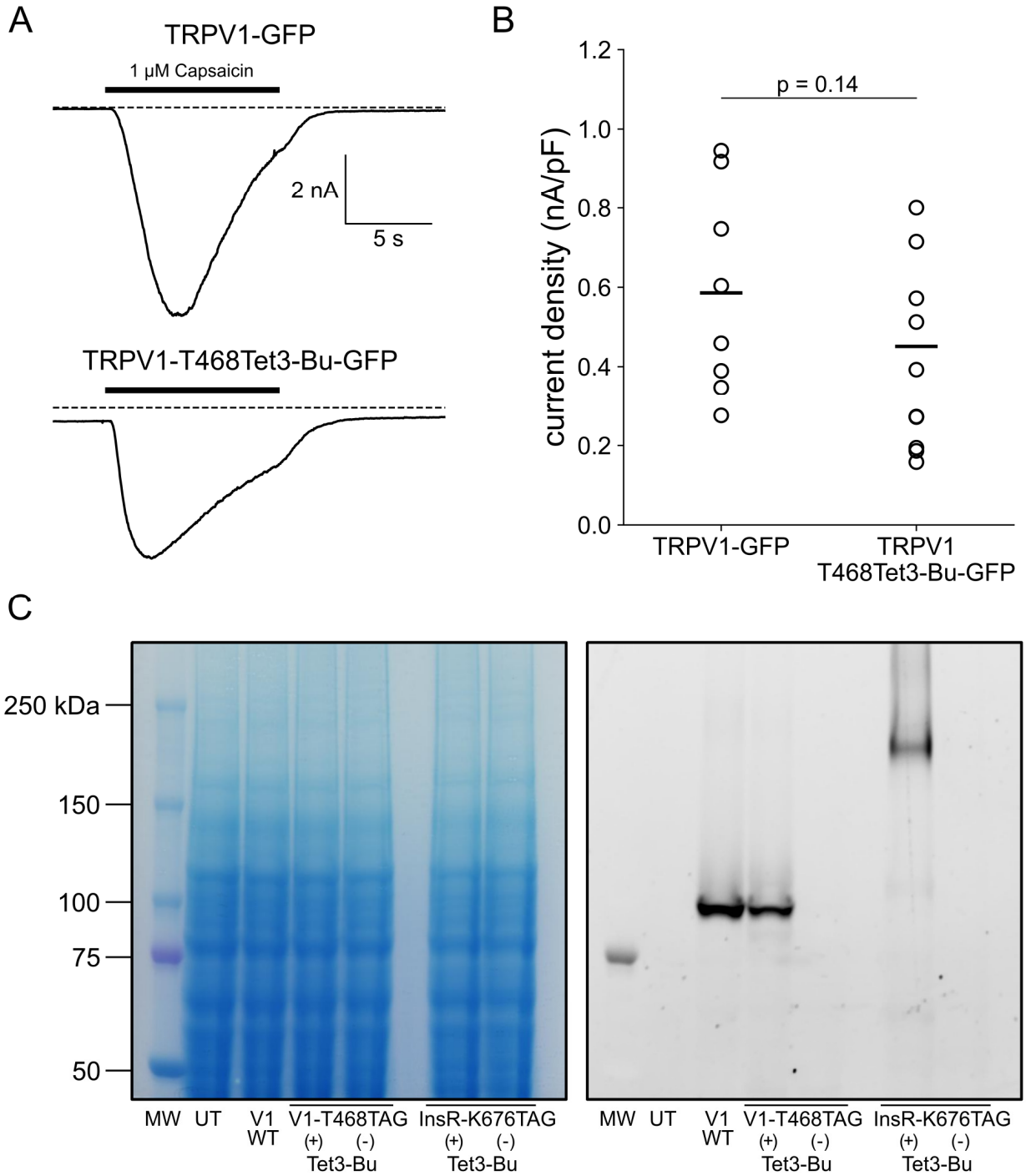

Figure 3-fig. supp. 1

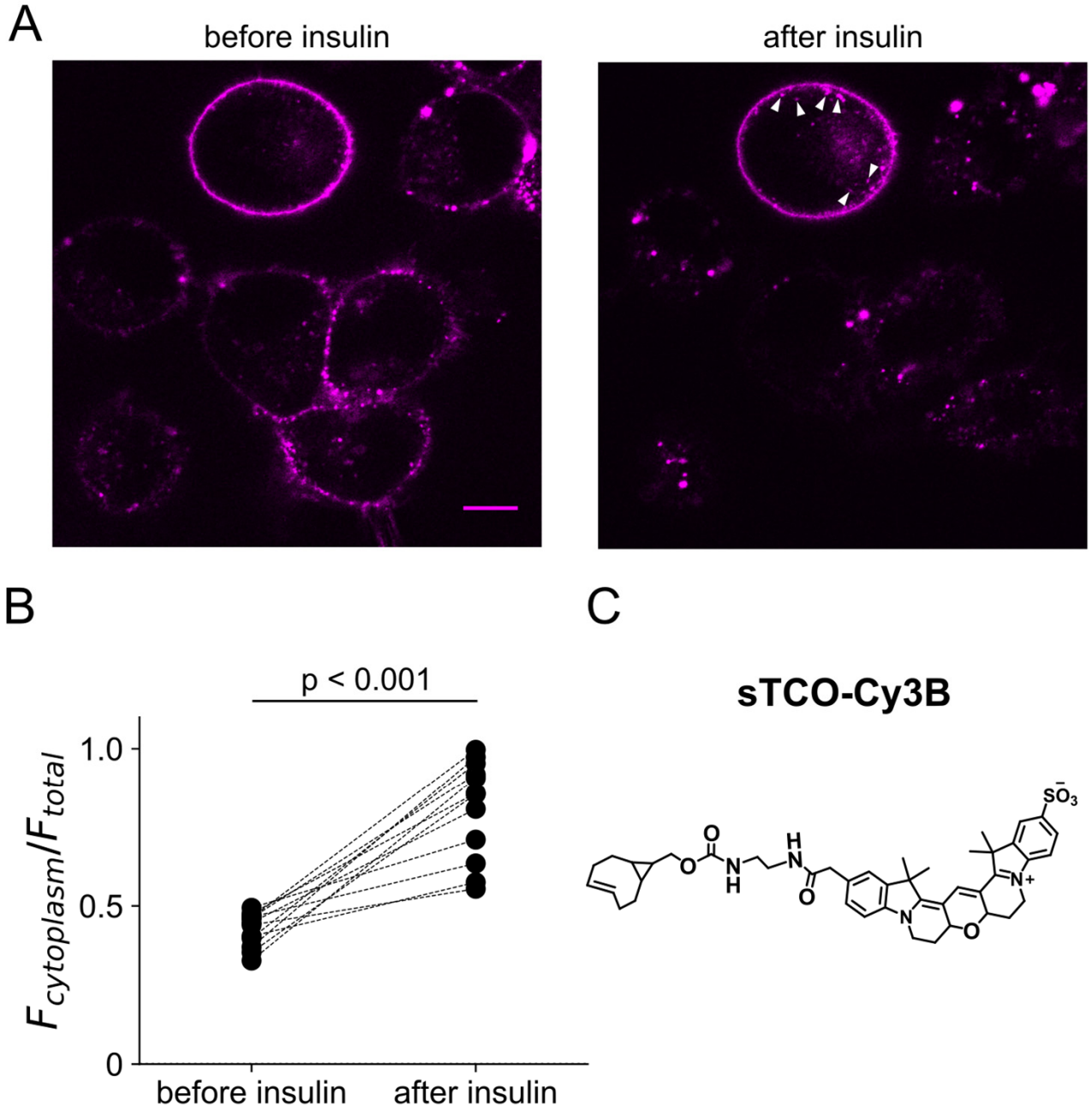

Figure 3-fig. supp. 2

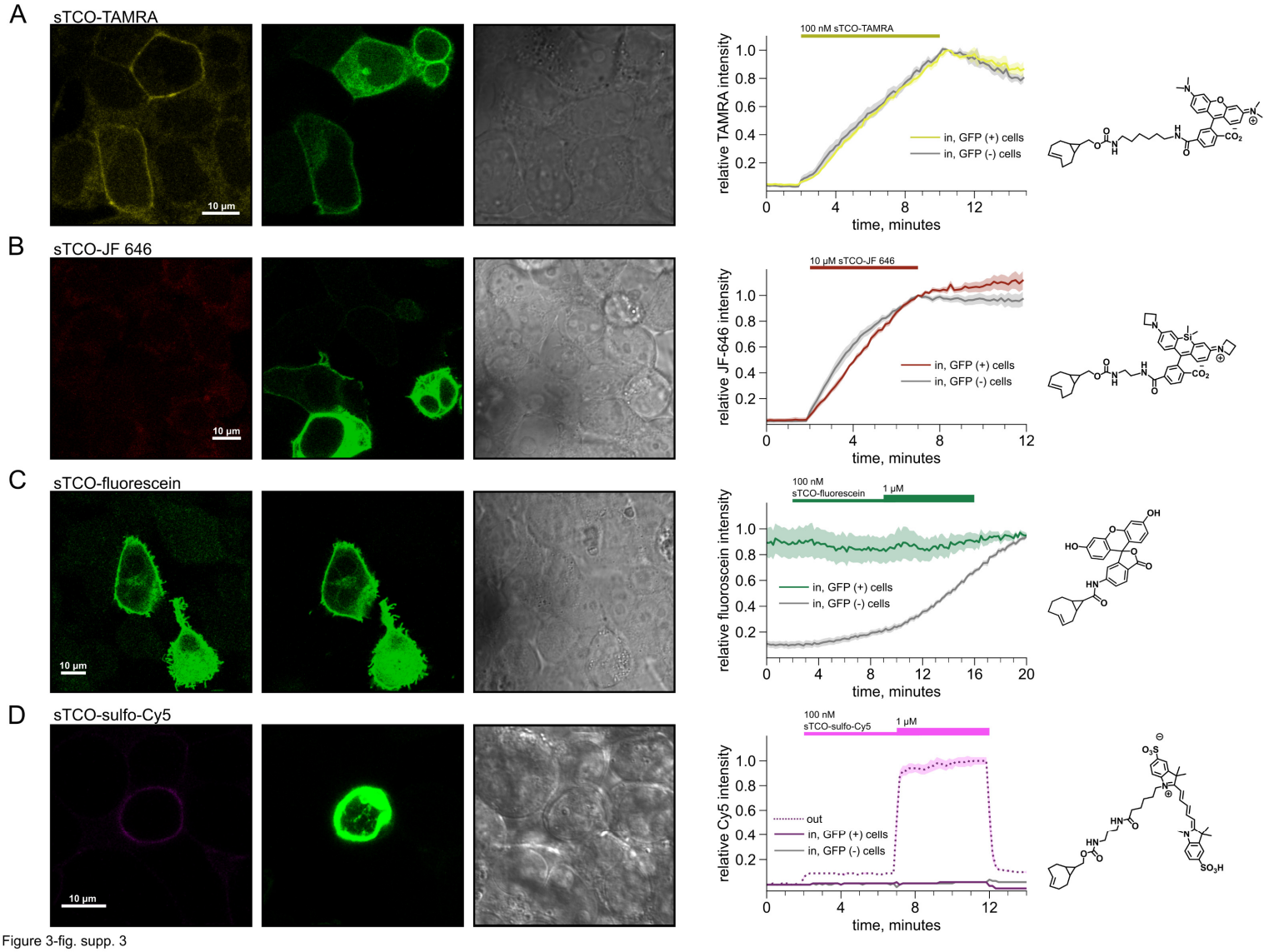

Figure 3-fig. supp. 3

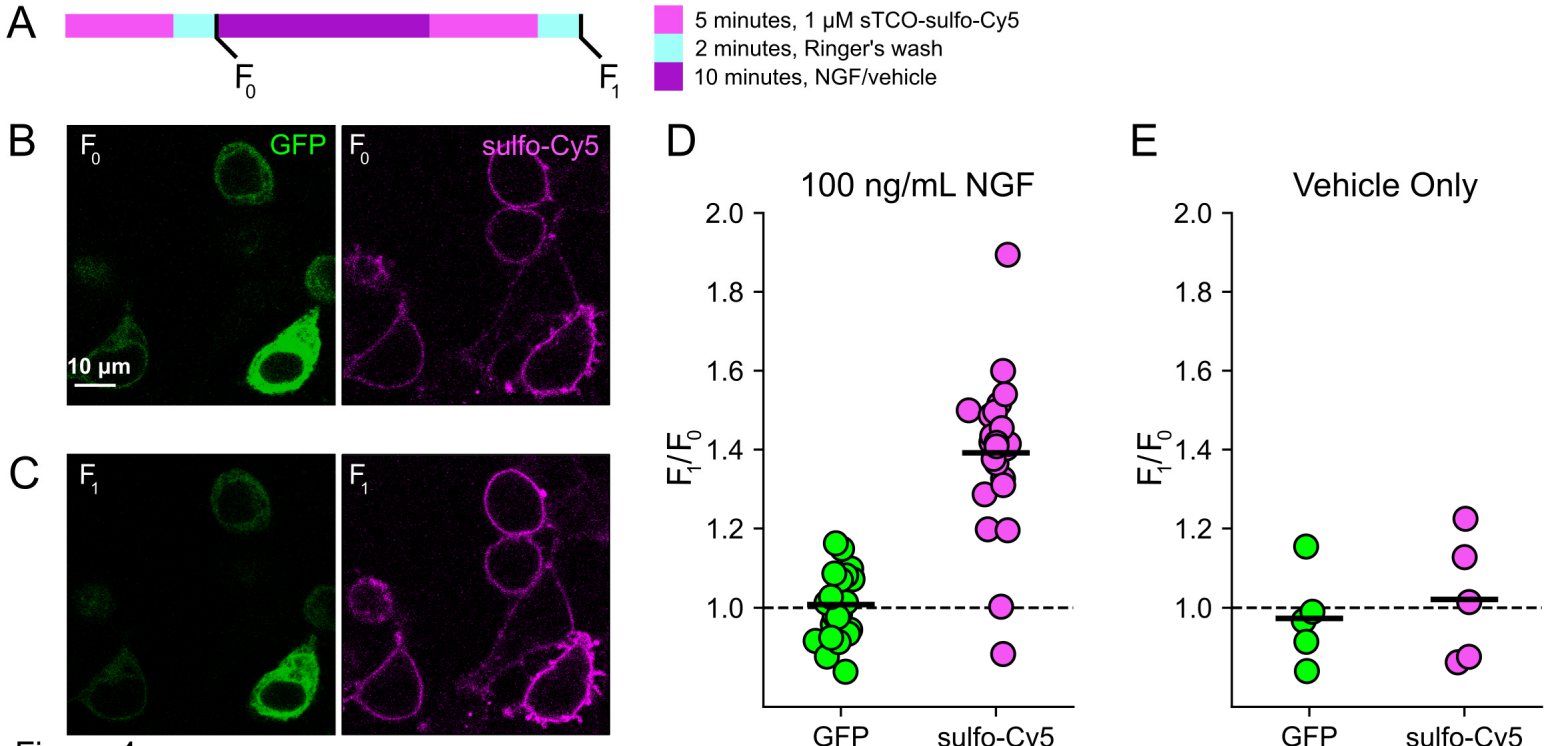
A
F0
F1
5 minutes, 1 μM sTCO-sulfo-Cy5
2 minutes, Ringer's wash
10 minutes, NGF/vehicle
B
F0
GFP
F0
sulfo-Cy5
10 μm
C
F1
F1
D
100 ng/mL NGF
2.0
1.8
1.6
1.4
1.2
1.0
F1/F0
GFP
sulfo-Cy5
E
Vehicle Only
2.0
1.8
1.6
1.4
1.2
1.0
F1/F0
GFP
sulfo-Cy5

Figure 4

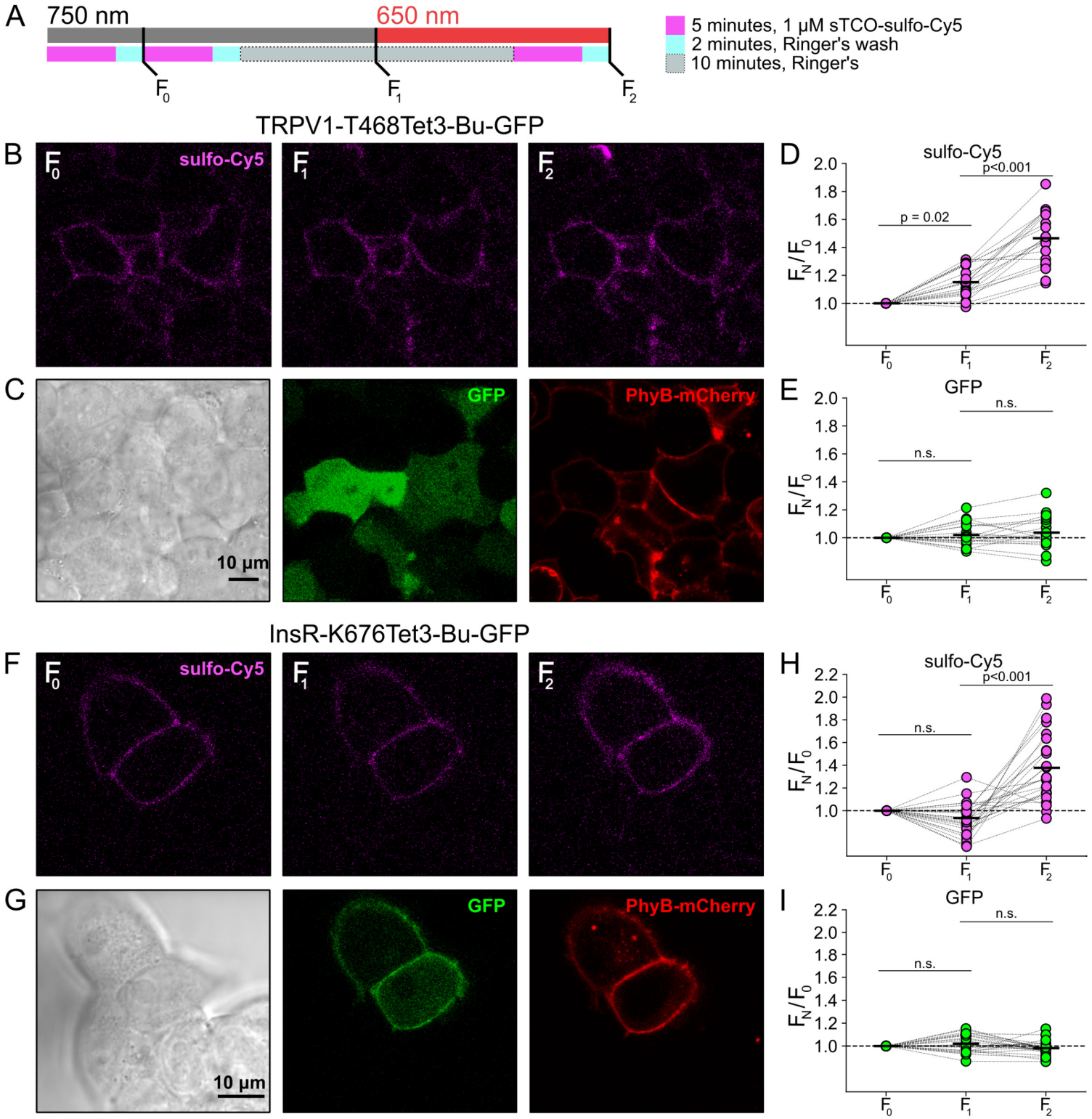
A
750 nm
650 nm
5 minutes, 1 µM sTCO-sulfo-Cy5
2 minutes, Ringer's wash
10 minutes, Ringer's
F0
F1
F2
TRPV1-T468Tet3-Bu-GFP
B
sulfo-Cy5
C
GFP
PhyB-mCherry
10 µm
D
sulfo-Cy5
p<0.001
p = 0.02
FN/F0
E
GFP
n.s.
InsR-K676Tet3-Bu-GFP
F
G
H
I

Figure 5

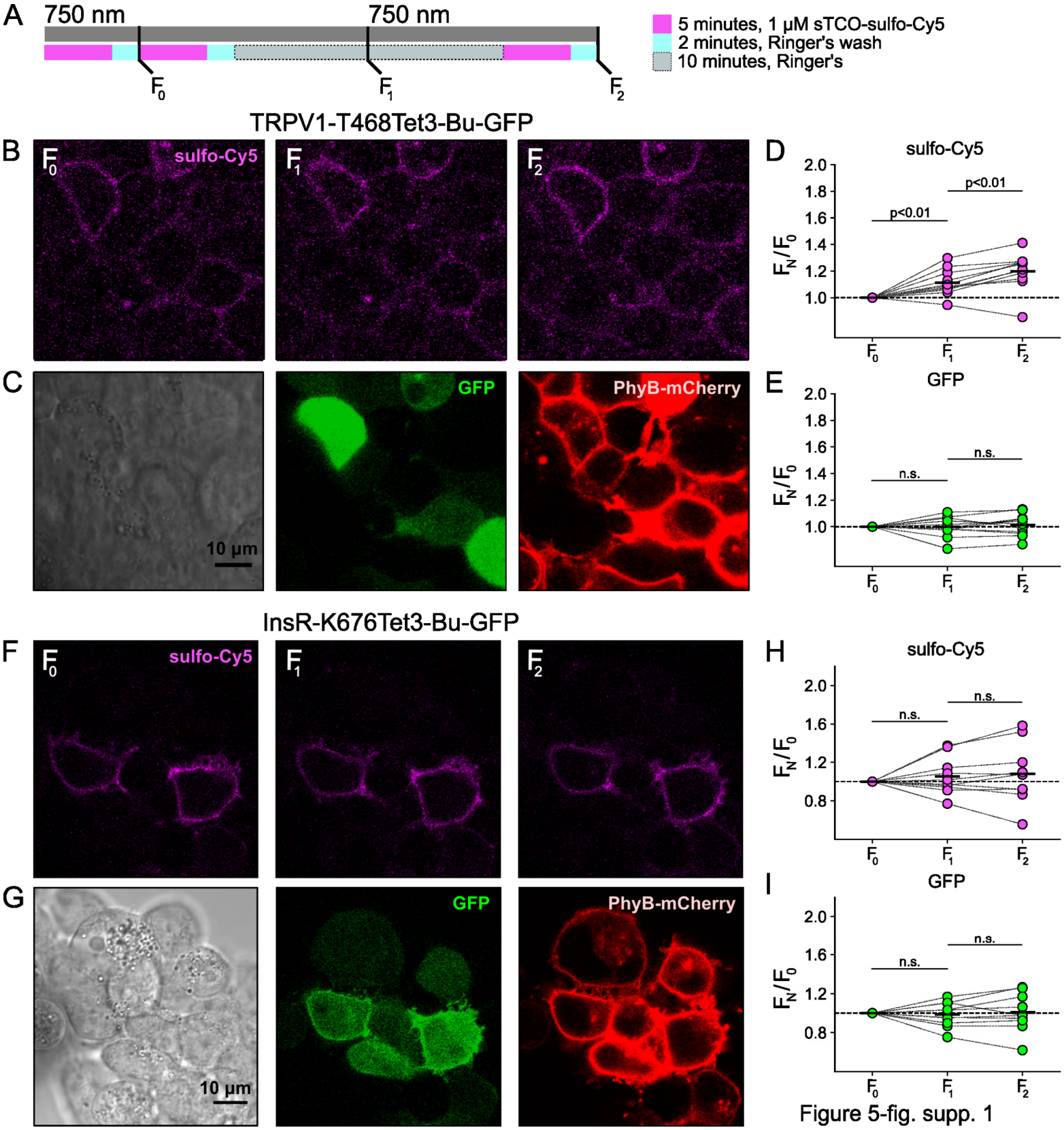

Figure 5-fig. supp. 1

A

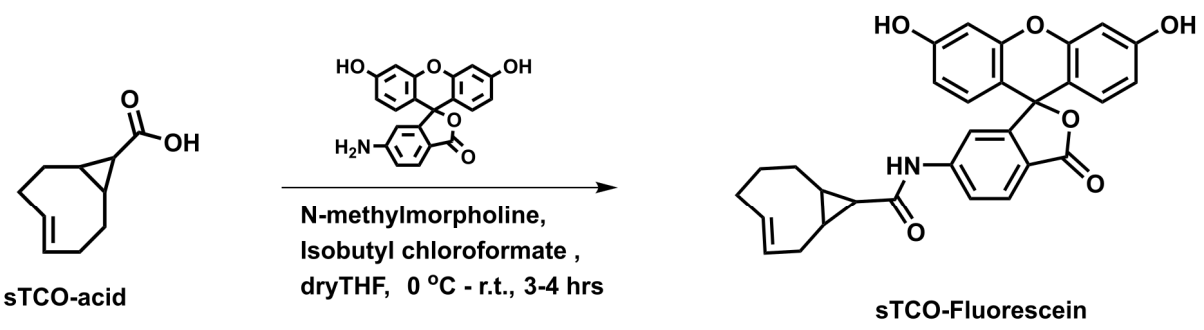
sTCO-acid
N-methylmorpholine,
Isobutyl chloroformate ,
dryTHF, 0 °C - r.t., 3-4 hrs
sTCO-Fluorescein

B

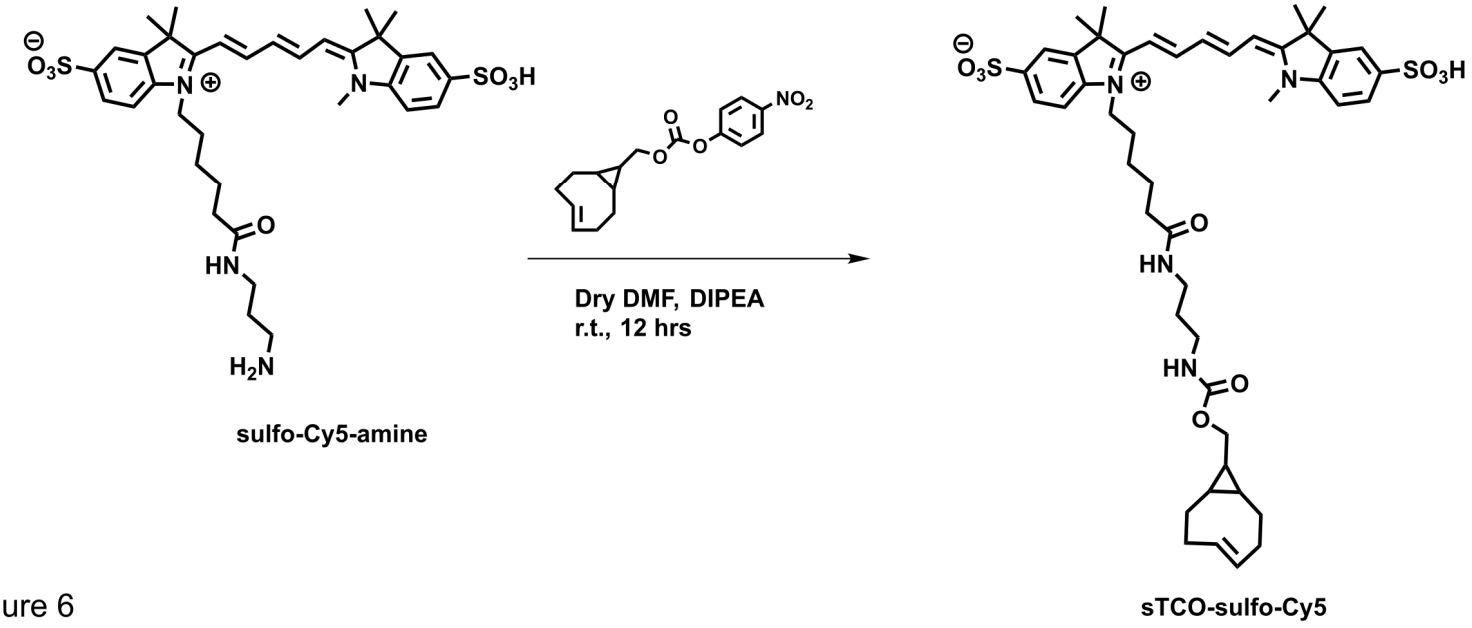
sulfo-Cy5-amine
Dry DMF, DIPEA
r.t., 12 hrs
sTCO-sulfo-Cy5

Figure 6

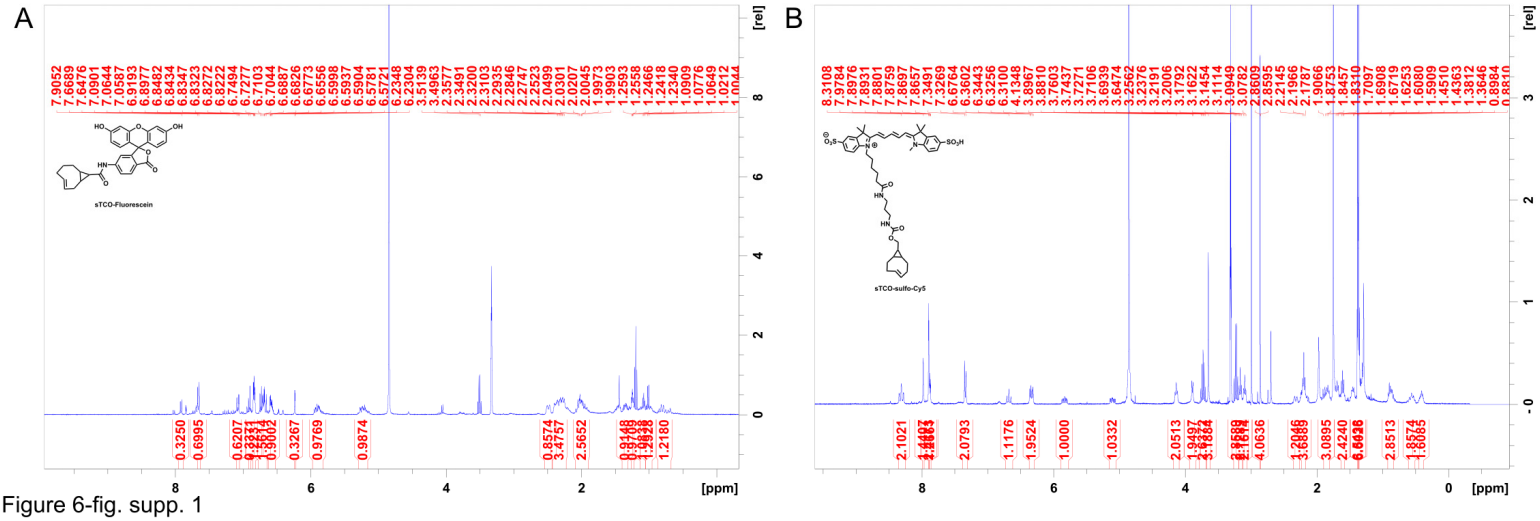

Figure 6-fig. supp. 1